

Examination of shoulder muscles' activity during a baseball pitch using musculoskeletal modeling

By

Zofia Agnieszka Tyczyńska, BSc. Automatic Control and Robotics

in partial fulfillment of the requirements for the degree of

Master of Science
in Mechanical Engineering

at the Delft University of Technology,
to be defended on 21.02.2023

Supervisors:

Prof. dr. H.E.J. Veeger, TU Delft
A.J.R. Leenen, MSc, VU Amsterdam

Contents

1	Introduction	1
2	Method	2
2.1	Experimental data collection	2
2.1.1	Participants	2
2.1.2	Procedure	3
2.1.3	Data acquisition	3
2.2	Model of the human shoulder	3
2.2.1	Scaling of the model	3
2.3	Performed analysis	4
2.3.1	Motion data selection	4
2.3.2	Inverse kinematics	4
2.3.3	Kinematic data analysis	4
2.3.4	Static optimization	5
2.3.5	Force and torque calculation	6
2.4	Model validation	6
2.4.1	Contribution of the coordinate actuators	6
2.4.2	EMG	7
3	Results	7
3.1	Data acquisition - data filtering	7
3.2	Kinematic analysis	7
3.3	Muscle length	8
3.4	Muscle activation	10
3.4.1	Torque	11
3.5	Model validation	11
3.5.1	Contribution of the coordinate actuators	11
3.5.2	EMG	12
4	Discussion	15
4.1	Kinematic analysis	15
4.1.1	Horizontal abduction/adduction	15
4.1.2	Internal/External rotation	15
4.1.3	Summary	15
4.2	Muscle length	15
4.2.1	Pectoralis major	15
4.2.2	Rotator cuff	17
4.2.3	Summary	17
4.3	Muscle activation	17
4.3.1	Torque	18
4.3.2	Comparison between participants	18
4.3.3	EMG data	19
4.3.4	Summary	19
4.4	Recommendations	20
4.4.1	Motion data collection	20
4.4.2	Model development	20
4.4.3	EMG data collection	21
5	Conclusion	21
5.1	Recommended improvement in OpenSim and Thoracoscapular Shoulder Model	22
A	Markers placement	25
B	OpenSim analyses	26
B.1	Model scaling	26
B.2	Muscle length	26
B.3	Fiber velocity calculation	30

B.4	Static optimization	30
B.4.1	Muscle activation	31
B.4.2	Torque	34
B.4.3	Coordinate actuators	38
B.4.4	Changes in pectoralis major length	41
C	Acceleration alignment	45
C.1	PP01	45
C.2	PP03	46
C.3	PP12	48
C.4	PP14	49
C.5	PP15	51

Abstract

A baseball pitch is an explosive and dynamic motion during which one of the highest angular rates achieved by the human body in sports activity was noted. The nature of the baseball pitch puts shoulder structures at risk, and one of the most common injuries among pitchers is a rotator cuff tear, frequently connected with internal impingement. It has been found that the amount of internal impingement increases for the angle of horizontal abduction beyond the coronal plane. To better understand the mechanics in the shoulder that leads to excessive horizontal abduction, it was decided to study muscle behavior (activation and produced torque) during the acceleration and deceleration phases of a baseball pitch. The study focused on muscles that are believed to have the most significant contribution during the aforementioned phases: pectoralis major and rotator cuff muscles (infraspinatus, supraspinatus and teres major). The analysis was performed with the use of the Thoracoscapular Shoulder Model [32] implemented in OpenSim software. About 20 pitches of 5 different baseball pitchers were simulated based on the collected marker motion data. Visible differences in the horizontal abduction/adduction angle were found between participants, with the angle of horizontal abduction between -10° to 18° at the moment of maximal external rotation (MER). Next, the muscle length was analyzed. The normalized muscle length of the rotator cuff muscles at MER was found to be similar to one found in the literature, as well as the changes in muscle length over time. However, discrepancies were found in the pectoralis major behavior. The conclusion was drawn that the thoracic part of the pectoralis major is too long. Moreover, it was found that the pectoralis major does not wrap around the humeral head and shaft for the horizontal abduction angle exceeding daily-live tasks. Next, static optimization was done to find the activation of the muscles in the glenohumeral joint and, consequently, to calculate the contribution of the individual muscles to the total torque in the joint. The contribution of the rotator cuff muscles was in accordance with the information found in the literature. However, the pectoralis major was not as active as expected. Instead of it, high activity of the deltoideus muscle and coordinate actuators was found. The results indicate that the pectoralis major was not working as expected, and other muscles needed to compensate for its normal function. Several improvements to the model and data collection were proposed. For the model development, it is suggested to ensure wrapping around the humeral head and shaft for the pectoralis major. Moreover, further evaluation of the model scaling is recommended, as problems with scaling the thoracic part of the pectoralis major were found. It is believed that after their implementation, it will be possible to find a potential correlation between the range of horizontal abduction and muscle activity while using the methodology and tools presented in this study.

1 Introduction

A baseball pitch is an explosive and dynamic motion during which one of the highest angular rates achieved by the human body in sports activity was noted [5]. The pitching motion consists of six phases: wind-up, stride, arm cocking, arm acceleration, arm deceleration, and follow-through (see Figure 1). The phases are divided by specific events in pitching, of which two are related to the position of the shoulder: maximal external rotation (MER) and maximal internal rotation (MIR). These two moments frame the acceleration and deceleration phases. The acceleration phase begins at the moment of MER and finishes with ball release (BR), and then the deceleration phase starts. The deceleration phase finishes at the moment of MIR. The acceleration and deceleration phases are thought to play the most significant role in upper limb injury development [5]. The internal rotation of the arm during those phases often exceeds 180° [10]. Furthermore,

Rotator cuff tears are the most frequent injuries of baseball pitchers [7, 28]. One of the possibilities of how the rotator cuff is damaged is its entrapment between the glenolabral complex and the humeral head, namely internal impingement [7, 14, 17]. Although internal impingement is a physiological phenomenon, it can become pathological [14, 24, 37] and cause rotator cuff and labrum tears [34]. The occurrence of internal impingement is often connected with the hyperangulation phenomenon [2, 24, 37]. The hyperangulation happens when, in a position of external rotation, a humerus is extremely horizontally abducted with respect to the glenoid [8]. During a baseball pitch, that can happen in the moment of MER, at the beginning of the acceleration phase. The range of horizontal abduction/adduction movement of the arm during the pitching motion exceeds 90° [10] and can be different between pitchers. Moreover, Mihata et al. [25] examined the influence of horizontal abduction on the amount of internal impingement and the pressure in the posterior-superior quadrant of the glenoid. They performed a study on cadaver shoulders. The results, however, may be inaccurate as the muscle dynamics had to be estimated. There is a possibility that the in vivo study might yield slightly different results. The conclusion from the experiment was that horizontal abduction beyond the coronal plane increases the amount of internal impingement.

The goal of the baseball pitch is to throw a ball such that the batter can not hit it. One option is to throw a fastball. In a fastball, the pitcher throws as fast as possible, and the energy is transferred to the ball during the acceleration phase through the throwing arm [6]. The trajectory of the arm and muscles' contribution

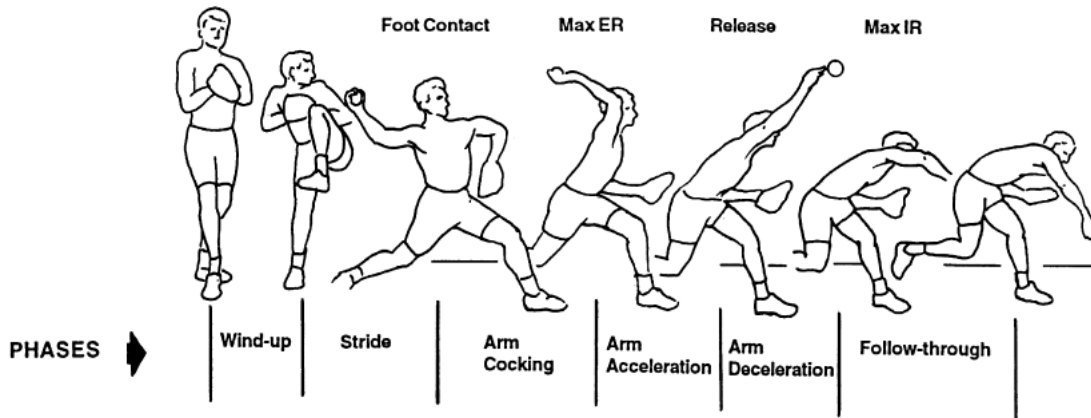


Figure 1: Phases of the baseball pitching motion: wind-up, stride, arm cocking, arm acceleration, arm deceleration, and follow-through. Adapted from Fleisig et al. [12]

should lead to the most optimized movement, as any deficits in the movement can lead to injuries and reduced performance [6]. To prevent injuries, it is crucial to understand how the motion considered harmful occurs. It was decided to focus on the horizontal abduction of the shoulder, which, while in an excessive range, can lead to the creation of rotator cuff tears. During the acceleration phase, the arm is horizontally adducted and internally rotated [11], though the range of the movement can be different between participants. The main sources of the differences between the movement of the players are muscle development and pitching technique. Though, differences in the pitching technique probably can also be noticed in the muscle behavior, as the changes in the pitching technique influence the kinematic parameters of the motion. Therefore, the main focus of this research is to describe the estimated muscle activity and the range of horizontal abduction. Escamilla and Andrews [11] and Mlynarek, Lee, and Bedi [27] analyzed muscle contribution during pitching motion phases. Based on the analysis made in the aforementioned papers, the following muscles were identified as having the biggest contribution to horizontal abduction/adduction movement: pectoralis major and rotator cuff muscles (supraspinatus, infraspinatus, and teres minor). The difference in those muscles' activity and the torque produced by them can influence the range of the horizontal abduction during the pitching motion [20, 37].

The goal of this paper is to examine the behavior of the shoulder muscles during the baseball pitch. The term muscle behavior is understood as muscle activity and torque produced by said muscles. The pitches of the several participants with different ranges of movement are analyzed. Identification of the relationship between muscles' behavior and the range of the horizontal abduction can help to identify muscles that should be of greater focus during training to prevent the occurrence of injury. Muscle activity can be investigated using surface electromyography (EMG). However, this method would not give complete insight into the forces and, consequently, torques produced by muscles during motion. Additionally, it can be challenging to gather data from all muscles of interest simultaneously, and not all parts of the muscle can be examined at the same time. However, the desired parameters can be obtained in another way, namely by using musculoskeletal modeling. With this approach, all required analyses can be performed based on experimental marker data, aided by modern musculoskeletal models and software tools. The EMG measurement can be used to validate the results obtained from the musculoskeletal models.

2 Method

2.1 Experimental data collection

2.1.1 Participants

15 male baseball pitchers took part in the following experiment. The age of participants was between 17 and 44 years old, with an average of 24.4 and a standard deviation (SD) equal to 7.5 years, an average mass of 79.4 kg and an SD of 9.4 kg, and an average height of 191 cm and an SD of 5cm.

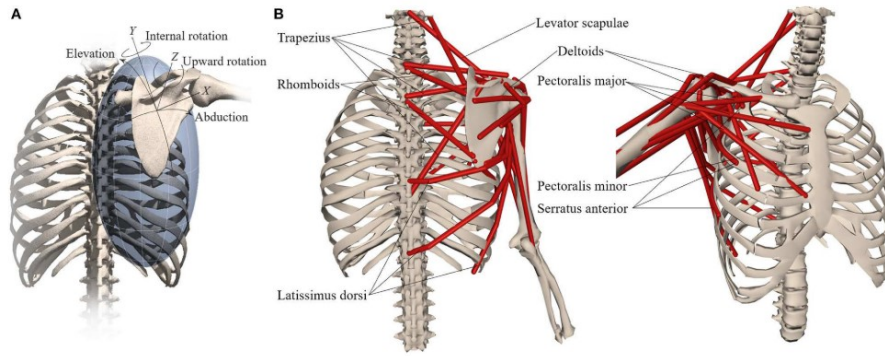


Figure 2: Musculoskeletal model with (A) scapula degrees-of-freedom and (B) shoulder muscles that control the scapula. Adapted from Seth et al. [32]

2.1.2 Procedure

The measurements were performed at the indoor facility of the Vrije Universiteit Amsterdam. Nine reflective markers were attached to the anatomical body landmarks using double-sided tape. The placement of the markers is presented in the [Appendix A](#). The participants wore their own shoes, athletic shorts, and glove but no shirts. The EMG electrodes were placed on the skin of the throwing arm and thorax. To enable synchronization of the EMG measurement with motion data, the accelerometer was located on the thorax below the incisura jugularis.

First, participants performed their regular warm-up, and then they were instructed to pitch fastballs with full effort. Ten fastball pitches were performed within a block of pitches, with two minutes of rest between each block. Each of the participants performed between 70 and 80 pitches. Participants pitched from a pitching mound (height 0.55m) towards a strike zone (height 0.71m; width 0.43m) at 18.66 m.

2.1.3 Data acquisition

The marker data were collected using a 3D motion capture system with 12 infrared cameras (Flex 13 Optitrack, Natural Point) and a sampling frequency of 120 Hz. The muscle activity was collected using bipolar surface Electromyography (sEMG). The following muscles were measured: Pectoralis Major Clavicular part (PC) and Sternal part (PC), Deltoideus (DM), and Latissimus Dorsi (LD). The electrode locations were based on the SENIAM guidelines [13]. In the measurement, disposable bipolar electrodes (Ag-AgCl; 1 cm² recording area; Blue Sensor Electrodes N-00-S, Ambu Inc.) were used. Electrodes were connected to a BioPlux device (Plux biosignals). In addition to the signal from electrodes, the BioPlux device was connected to one channel of the accelerometer (Plux biosignals). Data were gathered with a frequency of 2000 Hz.

2.2 Model of the human shoulder

A model with a complex shoulder structure with the scapula included is required to perform all desired analyses, including inverse kinematics and static optimization, to calculate muscle activity. The model needs to contain all muscles of interest: pectoralis major and rotator cuff muscles (supraspinatus, infraspinatus, and teres minor). It was decided to use Thoracoscapular Shoulder Model [32] (see [Figure 2](#)). The Thoracoscapular Shoulder Model has 11 DoF (see [Table 1](#)), plus 6 DoF between thorax and ground (3 rotations and 3 translations).

2.2.1 Scaling of the model

Model scaling was performed in two steps:

- Static (geometric) scaling of the model using Scaling Tool from OpenSim 4.3 software [9, 33]. Detailed data about how the scaling ratio was calculated are presented in [Appendix B](#). The scaling tool adjusts not only the size of the bones in the model but also the optimal length of the muscles and tendons.
- Optimization of the position of the markers in the model using sample dynamic motion. This was done using the Inverse Kinematics Tool from OpenSim software. The goal of the optimization was to minimize the weighted least squares equation of the position of the marker during motion. [9]

Both steps were performed using a MATLAB script created by Belli [1]. One of the crucial parts of the code is creating a set-up file for the Inverse Kinematics Tool. Belli has created a method to better approximate scapula

Table 1: Degrees of freedom of the Thoracoscapular Shoulder Model with corresponding joints

name of DoF	Model joint
clav_prot clav_elev	sternoclavicular joint
scapula_abduction scapula_elevation scapula_upward_rot scapula_winging	scapulothoracic joint
plane_elv shoulder_elv axial_rot	glenohumeral joint
elbow_flexion pro_sup	elbow

movement when not enough marker data are available. The experimental data set contains only one marker on the scapula, which allows the scapula to perform unnatural movements (e.g., flipping to an upside-down position for one frame). To limit this type of movement, some constraints on the scapula movement were added. These constraints limit the range of motion of the scapula between the frames, avoiding its unnatural behavior.

2.3 Performed analysis

Analyses performed on the model to obtain muscle data about muscle behavior are presented in the following section.

2.3.1 Motion data selection

First, the left-handed participants were eliminated from the dataset, as the model used in the study had only the right arm. Secondly, participants without a correctly captured static pose were also removed. The static pose data is assumed to be correctly captured when all markers of interest are visible for a minimum of 0.5 seconds. Next, pitches in which many markers were not visible were cut out. Finally, from the remaining data, around 20 first pitches per participant were chosen for the analysis.

2.3.2 Inverse kinematics

Inverse kinematics was performed with the use of the Inverse Kinematics Tool in the OpenSim GUI. As for scaling, the set-up was created using scapula constraints created by Belli [1]. The result of the inverse kinematics is the *Coordinate* file, describing the change of the model coordinates (DoFs) over time.

The results of the inverse kinematics were initially analyzed to ensure that model has a sufficient range of motion in the glenohumeral joint to perform baseball pitching. The Thoracoscapular Shoulder Model has the range of axial rotation between -75° and 75° while an observed range of external rotation for baseball pitchers can be even 180° [10]. The range of axial rotation was adjusted for each participant individually to enable the performance of the recorded motion.

2.3.3 Kinematic data analysis

The shoulder angles: abduction, horizontal abduction/adduction, and axial rotation, were defined using the rotation matrix describing the orientation of the humerus with respect to the thorax. The rotation order was described as X-Y-Z (shoulder abduction - horizontal abduction/adduction - internal/external rotation), and angles were calculated using the Euler decomposition.

Phases of a baseball pitch are distinguished by characteristic events. In this study, only two phases need to be distinguished: acceleration and deceleration phases. To do such following moments need to be identified: maximal external rotation (**MER**), ball release (**BR**), and maximal internal rotation (**MIR**). MER and MIR are the minimum and maximum of the axial rotation, respectively. BR does not have a strict kinematic definition and can therefore be obtained in several different ways how it can be obtained. In this study, it was chosen to define BR as the moment when the wrist overtakes the elbow in a forward direction [36].

Muscle lengths were extracted from the model motion. Fiber length was calculated using muscle length and the corresponding optimal tendon length by subtracting a later value from the first one. Next, based on the fiber

length, the shortening velocity was calculated. The obtained velocities have been filtered using a low-pass filter with a cut-off frequency of 12.5Hz.

During the geometric scaling of the model, muscle properties (including muscle optimal length) were scaled as well. Therefore, to make a comparison between participants easier, the lengths of the muscles are normalized (Equation 1). It can be interpreted that when $l_{normalized} < 1$, muscle is contracted, and when $l_{normalized} > 1$, muscle is stretched.

$$l_{normalised} = \frac{l}{l_{optimal}} \quad (1)$$

where: $l_{normalised}$ is normalized length of muscle; l is measured length of muscle and $l_{optimal}$ is optimal muscle length.

2.3.4 Static optimization

A static optimization tool can be used to calculate muscle activity during a given motion. The Static Optimization Tool available in OpenSim was not used because the joint constraints used in the Thoracoscapular Shoulder Model are not defined in the given tool. For that reason, a custom-made MATLAB script by Belli [1] was used to perform the static optimization. Contrary to the custom OpenSim optimization, the script by Belli does not approximate the model motion between frames, which can result in extremely high accelerations in the glenohumeral joint during the acceleration and deceleration phases. For that reason, data needed to be upsampled. Belli made an assumption that the acceleration in a given joint is a linear function of the muscle activation of muscles working in the given joint and that, consequently, muscle activation can be calculated using the generalized coordinates resulting from the inverse kinematics [1]. Equation 2 presents the cost function [1].

$$\min_{\mathbf{a}_k, \mathbf{c}_k} \sum_{i=1}^{N_m} w_i a_{i,k}^2 + \sum_{j=1}^{N_c} v_j c_{j,k}^2 \quad (2a)$$

$$\text{s.t.} \quad 0 \leq a_{i,k} \leq 1 \quad \forall i \in \mathbb{R}^{n_m} \quad (2b)$$

$$-1 \leq c_{j,k} \leq 1 \quad \forall j \in \mathbb{R}^{n_c} \quad (2c)$$

$$\mathbf{A}_{acc}[\mathbf{a}_k \ \mathbf{c}_k]^T = \ddot{\mathbf{q}} \quad (2d)$$

where $a_{i,k}$ and $c_{j,k}$ are activations of muscles and coordinates actuators, respectively, and w_i and v_j are their respective weights; \mathbf{A}_{acc} represents acceleration in the joint calculated based on the muscle activation and actuators signal; $\ddot{\mathbf{q}}$ is joint acceleration calculated using inverse kinematics.

Data upsampling

Because of the dynamic nature of the motion, especially visible during the acceleration phase, it was decided to upsample data from 60Hz to the frequency of 360Hz. The upsampling was performed on the Coordinate file, the result of the Inverse Kinematics. This was done using the spline function from MATLAB.

Modification of model maximal isometric force

The baseball pitching motion is extremely dynamic, and it is possible that muscles are acting close to their maximal activity. Because of that, it is important to ensure that the muscles of the model are sufficiently strong to perform a given task. Muscle properties of the Thoracoscapular Shoulder Model were estimated based on the shoulder of a 57-year-old muscular male [3, 32]. The participants of this experiment were young males. Therefore, muscle properties needed to be scaled. To do so, the maximal isometric force of the muscles was scaled, and it was decided to scale all muscles of the given participant with the same factor. To set a value of the scaling factor, it was gradually increased to the value that enables the model to perform baseball pitch, and no major activation changes occurred. For scaling factors greater than 3, only integers were used.

Coordinate actuators

Additionally, for modification of the isometric force, the joint actuators were added to model joints, one for every degree of freedom of the model. The detailed list of the actuators with their properties is presented in Appendix B. Including actuators allows for static optimization and satisfying acceleration constraints when the model muscles are not able to produce enough torque.

2.3.5 Force and torque calculation

Based on the muscle activity, the force produced by the muscles can be calculated. For the used muscle model, a force of the muscle can be presented as a linear function of muscle activation, as the activation dynamic of muscles was ignored (Equation 3) [26].

$$F_i = F_{A,i}x_i + F_{P,i} \quad (3)$$

where: $F_{A,i}$ is active force multiplier, x_i is function of muscle activation and $F_{P,i}$ is passive force multiplier. i iterates through all muscles in the model. Both $F_{A,i}$ and $F_{P,i}$ are calculated based on the muscles properties and state in any given moment (Equation 4 and Equation 5).

$$F_{A,i} = M_{f-vel,i} \cdot M_{f-len,i} \cdot F_{iso,max,i} \cdot \cos(\alpha_{p,i}) \quad (4)$$

$$F_{P,i} = F_{passive,i} \cdot F_{iso,max,i} \cdot \cos(\alpha_{p,i}) \quad (5)$$

where: $M_{f-vel,i}$ is an active force multiplier based on muscle force – velocity relation; $M_{f-len,i}$ is an active force multiplier based on muscle force – length relation; $F_{passive,i}$ is a passive force multiplier, for parallel elastic element; $F_{iso,max,i}$ is maximum isometric force and $\alpha_{p,i}$ is a pennation angle [30]. All mentioned multipliers are derived from the respective relations based on the muscle model described by Millard et al. [26]. $F_{iso,max}$ are based on the study by Breteler, Spoor, and Helm [3] and multiplied by the scaling factor described in the subsection 2.3.4.

Next, based on the obtained force and model kinematics, the torque in a joint can be calculated:

$$T_{i,c} = r_{i,c} \cdot F_i \quad (6)$$

where $T_{i,c}$ is torque in the joint from i muscles, around c axis, and $r_{i,c}$ is the moment arm of the given muscle to the corresponding axis.

Additionally, to simplify the analysis, the torque produced by individual muscle parts was added and presented as torque produced by the whole muscle. Next, to quantify the contribution of the individual muscles to the total torque in the total torque, the effective component was calculated. The method of computing the effective component is presented below (Equation 7 and Figure 3).

$$\cos(\alpha) = \frac{T_{sum} \cdot T_i}{|T_{sum}| |T_i|} \quad (7a)$$

$$c_{effective} = \cos(\alpha) \frac{|T_i|}{|T_{sum}|} \quad (7b)$$

where T_{sum} is the vector of the total torque in the joint; T_i is the vector of the torque produced by the individual muscle; α represents the angle between those two vectors and $c_{effective}$ is an effective component.

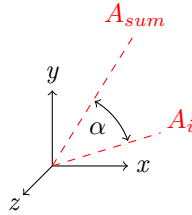


Figure 3: A_{sum} represents the axis around which total torque in the joint is working; A_i represents the axis corresponding to the individual muscle, and α is the angle between those two axes.

2.4 Model validation

2.4.1 Contribution of the coordinate actuators

The coordinate actuators were added to the model (see subsection 2.3.4), and their impact on the total torque in the joint should be minimal. The first step of the validation of the obtained muscles activation and torques is to check the contribution of the coordinate actuators. If they produce torque in the joint, the model is not strong enough to perform the required motion, and some modifications should be done.

2.4.2 EMG

The muscle activity calculated using static optimization can be validated with the use of the collected EMG data. First, the EMG data needed to be synchronized with the motion files. It was achieved by using the acceleration of the thorax (IJ marker) with respect to ground and data collected by the accelerometer. A more detailed description of the alignment can be found in [Appendix C](#).

Next, the absolute value of the measured EMG signal was taken, but no filtering or normalization was done. Any additional actions on the measured muscle activation were pointless as there is no connection between the muscle force of the OpenSim model and the measured strength of the participants. Therefore, validation has been done by comparing if the given muscle has been active at the same time. Additionally, measured muscle activity was compared with muscle shortening velocity.

3 Results

3.1 Data acquisition - data filtering

The criteria used to filter the motion data led to the following results:

- 4 participants were left-handed and were eliminated in this stage;
- 6 participants were not correctly captured during the static phase.

As a result, 5 participants were left for further analysis. The age of participants was between 20 and 26 years old, with an average of 23.4 and an SD equal to 2.4 years, an average mass of 77.4 kg and an SD of 6.5 kg, and an average height of 193 cm and an SD of 5cm.

3.2 Kinematic analysis

Next, the kinematics of the model were analyzed. This research focuses on the influence of horizontal abduction on the behavior of muscles. Because of that, the primary focus was to analyze shoulder behavior. The difference in the range of motion of the participants has been presented in [Table 2](#). Additionally, the angle of axial rotation, abduction, and horizontal abduction at MER were presented in [Table 2](#). The angles in the thoracohumeral joint (angles between the thorax and humeral) over pitching time for all participants are presented on [Figure 4](#). As can be seen, all participants repeat the pitching motion in the same way, with a low standard deviation. Participant 12 did not cross the plane of the thorax at MER, with the humeral still horizontally adducted, for the rest of the participants' horizontal adduction between around 0° to 20° can be observed.

Table 2: Comparison between participants: range of axial rotation and angles in the shoulder at MER. Presented values are the average and standard deviation of 20 pitches.

participant	range of axial rotation [°]	values at MER			visualisation
		axial rotation [°]	horizontal adduction [°]	abduction [°]	
PP01	-180 - 40	-177.08 ± 1.55	-1.03 ± 1.05	78.83 ± 1.46	
PP03	-150 - 40	-148.47 ± 0.86	-9.95 ± 0.77	87.77 ± 1.48	
PP12	-140 - 40	-139.33 ± 0.69	10.68 ± 0.72	82.6 ± 1.08	
PP14	-150 - 40	-144.26 ± 3.87	-18.69 ± 2.75	80.16 ± 1.87	
PP15	-160 - 40	-152.73 ± 1.73	-16.42 ± 1.38	76.74 ± 0.96	

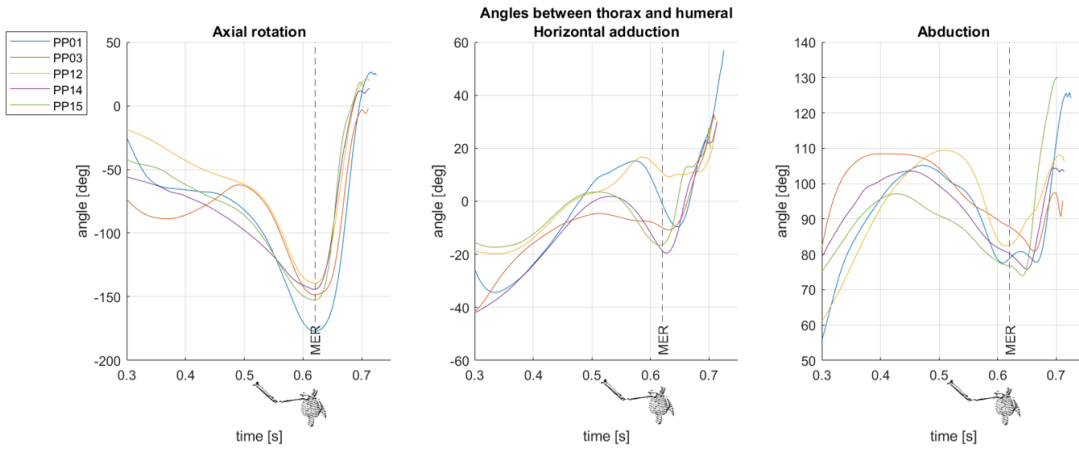


Figure 4: Comparison of Euler angles between the thorax and humeral for all participants. The left plot: for the axial rotation, the internal rotation is with positive values, and the external rotation for negative values. For the central plot: the arm is horizontally adducted for positive values and abducted for negative. The right plot presents shoulder abduction, with positive values representing the angle of shoulder abduction. Presented values are an average of approximately 20 pitches for each participant.

3.3 Muscle length

Next, based on the kinematic data, muscle length can be analyzed. In the [Figure 5](#) normalized length of the pectoralis major is presented for all participants (normalized muscle length for the rest of the muscles of interest is presented in [Appendix B](#)). Moreover, in the [Table 3](#) normalized muscle length in the moment of MER is compared with the results of Hordijk [16], data for more muscles can be found in [Appendix B](#) ([Figure 17](#) - [Figure 19](#)).

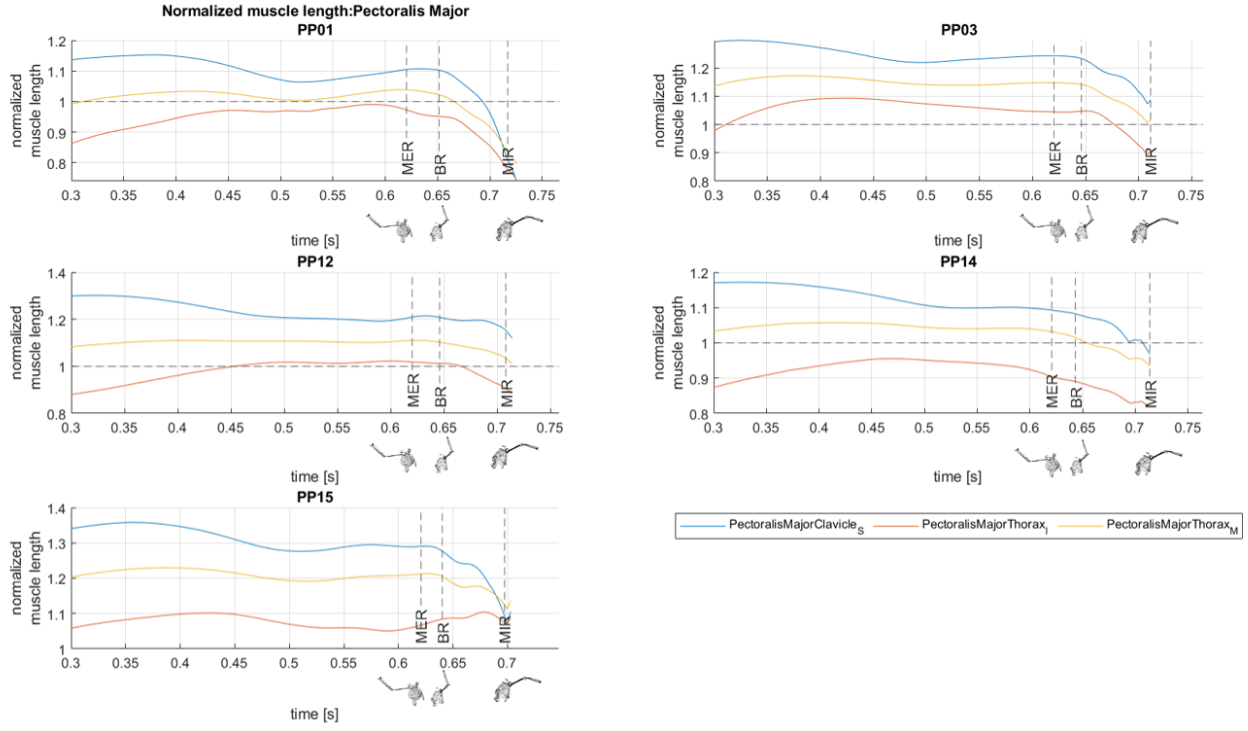


Figure 5: Normalized muscle length of pectoralis major during the pitching motion. Normalized muscle length = muscle length / optimal muscle length.

Table 3: Normalized muscle length (muscle length/optimal muscle length) at the moment of MER compared with results from Hordijk [16]. The red scale of color indicates that the normalized muscle length is shorter than expected, and the blue scale of color indicates that the muscle is longer than expected.

Muscle name	muscle length / optimal muscle length					group average	Hordijk [16]
	PP01	PP03	PP12	PP14	PP15		
PectoralisMajorClavicle_S	1.105 ± 0.004	1.243 ± 0.004	1.209 ± 0.004	1.093 ± 0.006	1.29 ± 0.004	1.188 ± 0.077	1.34 ± 0.01
PectoralisMajorThorax_I	0.972 ± 0.003	1.044 ± 0.002	1.018 ± 0.001	0.905 ± 0.01	1.067 ± 0.008	1.001 ± 0.057	1.37 ± 0.02
PectoralisMajorThorax_M	1.039 ± 0.001	1.148 ± 0.002	1.11 ± 0.002	1.032 ± 0.005	1.212 ± 0.004	1.108 ± 0.068	
TeresMajor	1.189 ± 0.003	1.127 ± 0.007	1.21 ± 0.003	1.211 ± 0.009	1.362 ± 0.039	1.22 ± 0.077	1.18 ± 0.04
Infraspinatus_I	1.079 ± 0.011	0.813 ± 0.008	0.805 ± 0.007	0.862 ± 0.035	1.005 ± 0.011	0.913 ± 0.11	0.44 ± 0.05
Infraspinatus_S	1.366 ± 0.008	1.195 ± 0.006	1.148 ± 0.005	1.19 ± 0.027	1.277 ± 0.009	1.235 ± 0.078	
Supraspinatus_P	1.01 ± 0.011	0.794 ± 0.006	0.756 ± 0.004	0.796 ± 0.029	0.933 ± 0.011	0.858 ± 0.097	0.76 ± 0.04
Supraspinatus_A	0.903 ± 0.012	0.724 ± 0.004	0.713 ± 0.003	0.718 ± 0.021	0.85 ± 0.01	0.782 ± 0.079	
Subscapularis_S	1.023 ± 0.007	1.14 ± 0.004	1.123 ± 0.004	1.162 ± 0.015	1.146 ± 0.007	1.119 ± 0.049	
Subscapularis_M	0.924 ± 0.011	1.123 ± 0.006	1.097 ± 0.01	1.157 ± 0.033	1.083 ± 0.019	1.077 ± 0.08	0.69 ± 0.04
Subscapularis_I	1.287 ± 0.007	1.402 ± 0.003	1.393 ± 0.003	1.391 ± 0.013	1.351 ± 0.006	1.365 ± 0.043	

The data shows that the clavicular part of the pectoralis major is the most extended one. For participants 3, 12, and 15, the normalized length at MER is greater than 1.2, while for participants 1 and 14, the normalized length is closer to 1 (between 1.09 and 1.1). The thoracic part of the pectoralis major is not stretched for all participants. As can be seen on Figure 5, the thoracic inferior part for some participants is contracted. Moreover, the infraspinatus muscle is near its optimal muscle length for most of the participants. The normalized length of supraspinatus at MER is between 0.7 and 0.8 for participants 3, 12, and 14 and between 0.85 and 1 for participants 1 and 15. The normalized length of teres major is between 1.9 and 1.36 for all participants, with an average of 1.22.

Additionally, the normalized length of the muscle, with respect to the coordinate angles of the glenohumeral joint, was evaluated. The relative length of the muscle has been plotted against the elevation plane coordinate of the glenohumeral joint at the elevation of 90° and axial rotation of 0° (Figure 6). Evaluation with respect to

remaining degrees of freedom is presented in [Appendix B](#). The pectoralis major is getting longer while horizontal adduction is increasing. However, apart from the clavicular part, the muscle is not stretched (normalized length is not higher than 1). The inferior thoracic part of the pectoralis major stays contracted for all participants in the entire range of movement.

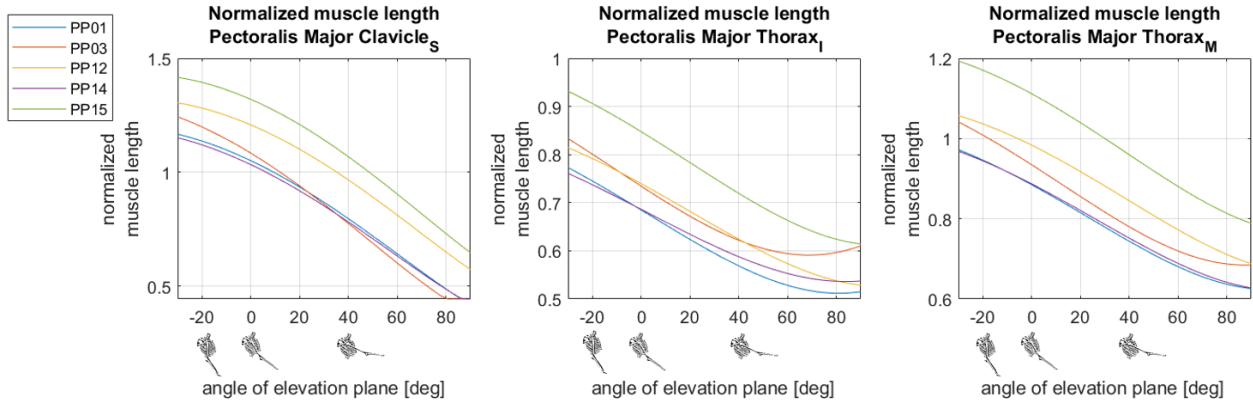


Figure 6: Normalized length (muscle length/optimal muscle length) of the pectoralis major with respect to the elevation plane coordinate of the glenohumeral joint. Comparison between participants. Shoulder elevation = 90° and axial rotation = 0° .

3.4 Muscle activation

Before performing the static optimization, the model's maximal forces were scaled. The final scaling factor used for all participants was decided to be 10. On [Figure 7](#), computed muscle activity of Pectoralis Major is presented. Results for other muscles of interest are presented in [Appendix B](#). For all participants, the thoracic inferior part of the pectoralis major is most active during the acceleration phase. However, none of the participant's pectoralis major muscle activity exceeds half of its possible activation. Moreover, for participants 1, 3, and 15, the muscle activity of the pectoralis major is close to zero.

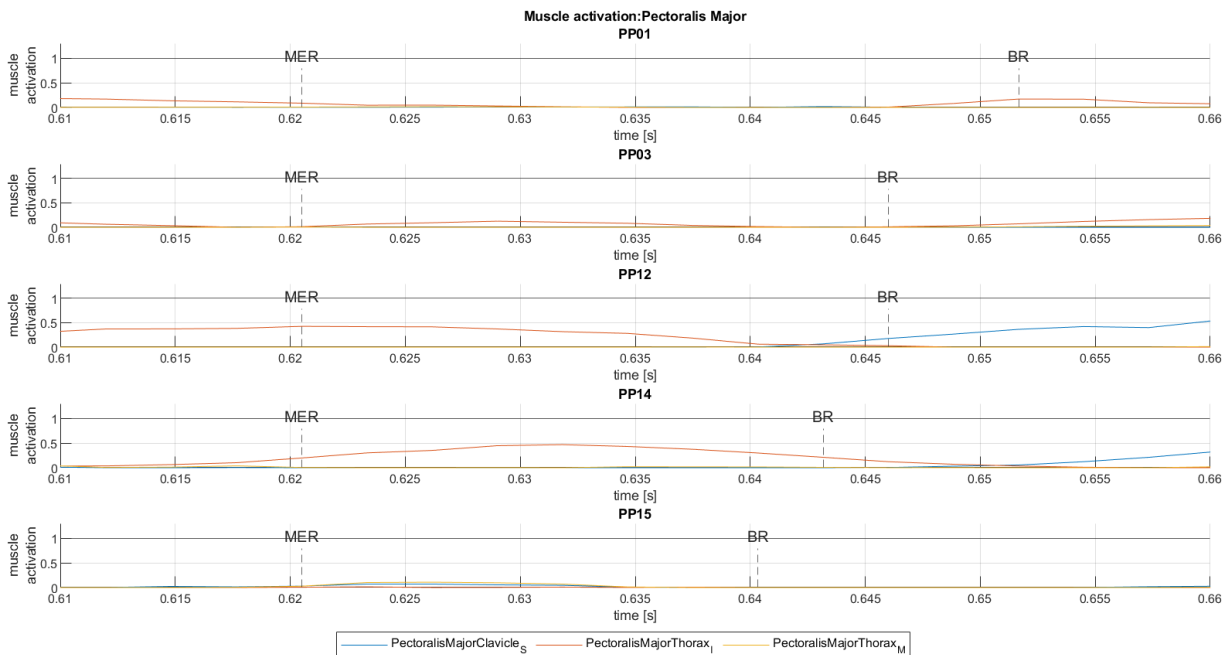


Figure 7: Muscle activity computed with the use of static optimization of Pectoralis Major during the acceleration phase.

3.4.1 Torque

The torque produced by individual muscle parts during the acceleration phase is presented in [Appendix B](#). In [Table 4](#) and [Figure 8](#), the torque produced by muscles at the moment of MER is presented. In [Table 5](#) and [Figure 9](#), the torque at BR is presented.

At MER, the deltoideus muscle contribution is the highest – in some parts of the acceleration phase, responsible for most of the produced torque (average of 0.5 among participants at MER). The deltoideus produces the torque needed for shoulder abduction and horizontal adduction (in the X and Y planes), and it has almost no contribution to axial rotation (in the Z plane). At BR, the contribution of the deltoideus muscle has decreased to 0.09 on average. The infraspinatus muscle has the biggest contribution to internal rotation motion, and its contribution decreases during acceleration motion. The contribution in the total torque from the infraspinatus is about 0.18 at MER and 0.09 at BR. The second biggest contribution during MER in the axial rotation plane is from the subscapularis muscle, its contribution increases during the acceleration phase, but it remains the second contributor at BR, as the contribution of the biceps is highest at BR. The biceps has the highest contribution to the torque in the axial rotation plane. However, it has as well the highest effective component at BR (0.55 on average). The contribution of the biceps increases during the acceleration phase as it is a muscle with the third highest effective components at MER (0.18 on average). Pectoralis major has, on average fifth biggest contribution at MER (about 0.07 of the effective component). At BR, pectoralis major has a smaller contribution (about 0.05 on average).

Table 4: Torque produced by muscles in the glenohumeral joint at MER

muscle name	PP01		PP03		PP12		PP14		PP15		group average	
	torque [Nm]	effective component	torque [Nm]	effective component								
Deltoideus	133.08	0.73	99.72	0.49	140.73	0.39	129	0.69	115.33	0.22	123.572	0.50
Infraspinatus	79.95	0.28	76.87	0.33	20.35	0.04	71.53	0.23	136.92	0.00	77.124	0.18
Biceps	42.7	0.05	38.11	0.10	148.2	0.24	52.99	0.04	124.18	0.30	81.236	0.15
TeresMajor	12.89	-0.07	8.58	-0.05	14.77	-0.05	14.77	-0.08	49.94	-0.13	20.19	-0.08
Pectoralis Major	6.99	0.01	26.46	0.10	23.16	0.07	16.15	0.06	28.73	0.10	20.298	0.07
Coracobrachialis	3.25	0.02	1.7	0.00	3.37	0.01	4.46	0.02	93.72	0.23	21.3	0.06
Supraspinatus	5.37	0.01	37.97	0.14	52.8	0.10	4.78	0.00	13.55	0.00	22.894	0.05
Subscapularis	3.77	-0.01	7.44	-0.02	7.93	0.00	8.21	0.00	62.6	0.08	17.99	0.01
Triceps long	0	0.00	0	0.00	1.47	0.00	1.92	-0.01	15.34	-0.04	3.746	-0.01
TeresMinor	3.05	0.00	0.07	0.00	0.14	0.00	7.44	0.01	15.19	0.00	5.178	0.00
Latissimus Dorsi	0.75	0.00	0	0.00	1.34	0.00	0	0.00	3.61	-0.01	1.14	0.00
coordinate actuators	5.68	0.02	2.68	0.00	38.43	0.12	0.98	0.00	13.55	-0.05	12.264	0.02

Table 5: Torque produced by muscles in the glenohumeral joint at BR.

muscle name	PP01		PP03		PP12		PP14		PP15		group average	
	torque [Nm]	effective component	torque [Nm]	effective component								
Biceps	92.87	0.75	137.24	1.3	120.21	-0.22	60.33	0.49	97.25	0.44	101.58	0.552
Teres Major	19.22	-0.2	30.72	-0.25	151.81	0.82	79.74	0.94	50.45	0.23	66.388	0.308
Triceps long	4.2	-0.04	0.27	0	89.08	0.53	18.06	0.19	31.97	0.16	28.716	0.168
Deltoideus	59.06	0.39	27.33	0.07	87.32	0.12	16.94	-0.17	7.52	0.04	39.634	0.09
Latissimus Dorsi	9.14	-0.09	4.07	-0.01	16.62	0.09	21.18	0.28	78.05	0.27	25.812	0.108
Subscapularis	5.38	-0.04	17.58	-0.12	60.54	-0.11	16.2	-0.23	43.75	-0.13	28.69	-0.126
Infraspinatus	21.88	0.3	6.31	0.04	0.3	0	5.21	0.04	10.19	0.07	8.778	0.09
Coracobrachialis	3.2	0.03	1.55	-0.02	2.99	-0.01	9.81	-0.07	61.28	-0.31	15.766	-0.076
Pectoralis Major	14.58	0.09	21.12	0.21	19.68	-0.02	20.19	0.01	19.75	-0.04	19.064	0.05
Supraspinatus	0	0	2.91	0.04	19.22	-0.12	11.41	-0.08	0.24	0	6.756	-0.032
Teres Minor	0.12	0	0.1	0	0	0	0.3	0	0.16	0	0.136	0
coordinate actuators	8.79	0.08	0.93	0	6.97	0.01	4.25	0.03	40.58	0.21	12.304	0.066

3.5 Model validation

3.5.1 Contribution of the coordinate actuators

In the [Figure 10](#), the group average of torque produced by the coordinate actuators. The figures for all participants separately can be found in [Appendix B](#). In the tables and plots presented in [subsubsection 3.4.1](#), the contribution of the coordinate actuators at the moment of MER and BR is also presented. From [Figure 10](#), it can be noticed that the group average of the torque produced by the coordinate actuator during the pitching

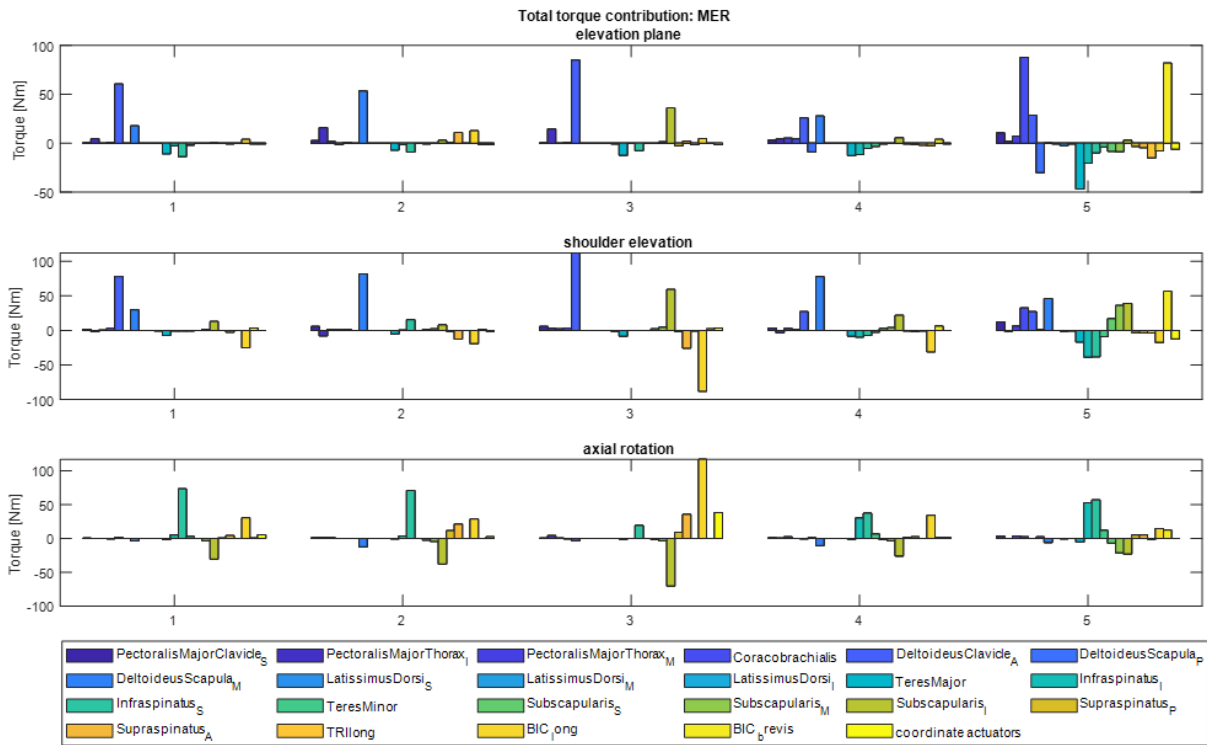


Figure 8: Torque produced by individual muscles at MER for all participants. 1 - PP01; 2 - PP03; 3 - PP12; 4 - PP14; 5 - PP15.

motion is close to zero and, for the most time, visibly lower than the total torque in the plane. The coordinate actuator has the highest contribution in the axial rotation plane, which can be as well seen in the [Figure 8](#) and [Figure 9](#). The noticeably high contribution of the coordinate actuator is at MER for participant 12 and at BR for participant 15. In the latter, the actuator produced the second-highest torque in the joint at the moment. Consequently, the coordinate actuator has the third highest contribution to total torque at BR for participant 15, 0.21, when the group average is about 0.07. The effective component of the total torque produced by the coordinate actuators for participant 3 is equal to 0 at both MER and BR. For participant 14, the effective component is equal to 0 and 0.03 at MER and BR, respectively.

3.5.2 EMG

Results of the alignment of the thorax acceleration are presented in the [Appendix C](#). In [Figure 11](#), synchronized data for the pectoralis major muscle of participant 1 are presented. Results for the rest of the measured muscles, as well as the rest of the participants, can be found in [Appendix C](#).

It can be noticed that data obtained from the OpenSim model are in accordance with each other, and muscle activation of the pectoralis major is observed when the muscle is shortening. However, it is not at the exact moment when higher muscle activity was measured. The clavicular part of the pectoralis major, according to the OpenSim simulation, is active during the acceleration and deceleration phases. When measured, EMG data show no activity during those phases. For participant 1 inferior thoracic part of the pectoralis major matches partially measured data, but for another is visibly different.

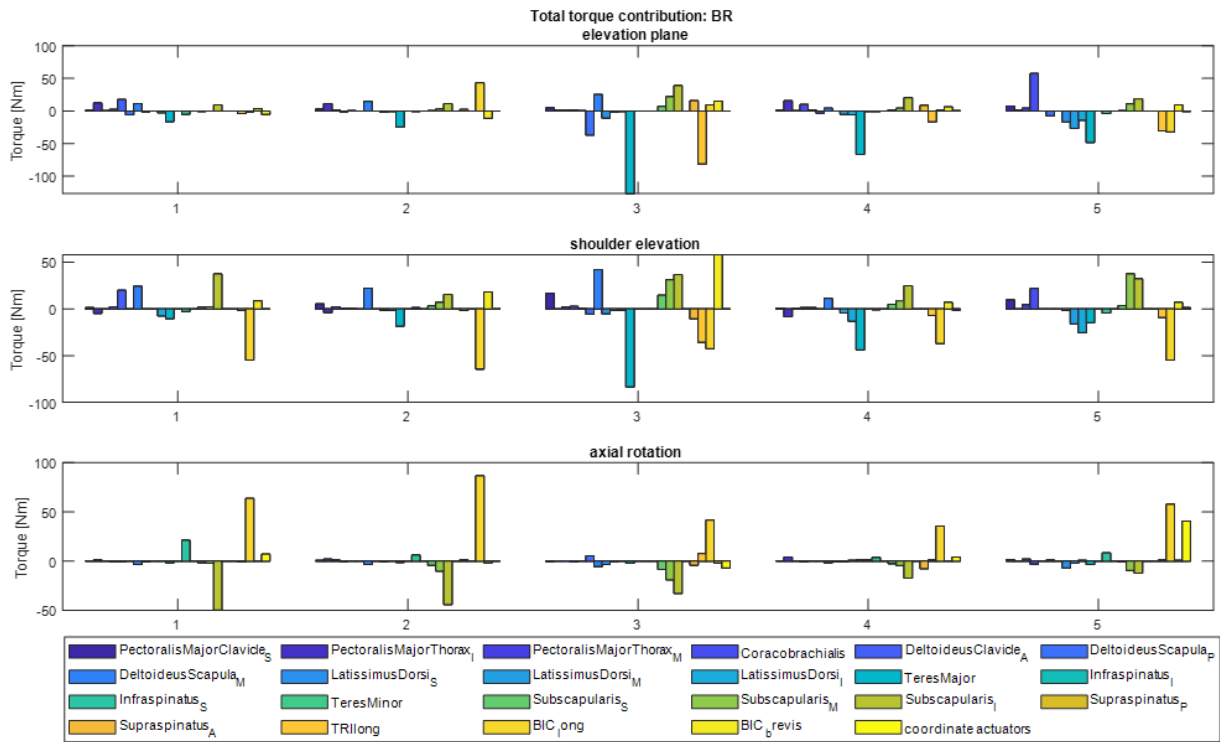


Figure 9: Torque produced by individual muscles at BR for all participants. 1 - PP01; 2 - PP03; 3 - PP12; 4 - PP14; 5 - PP15.

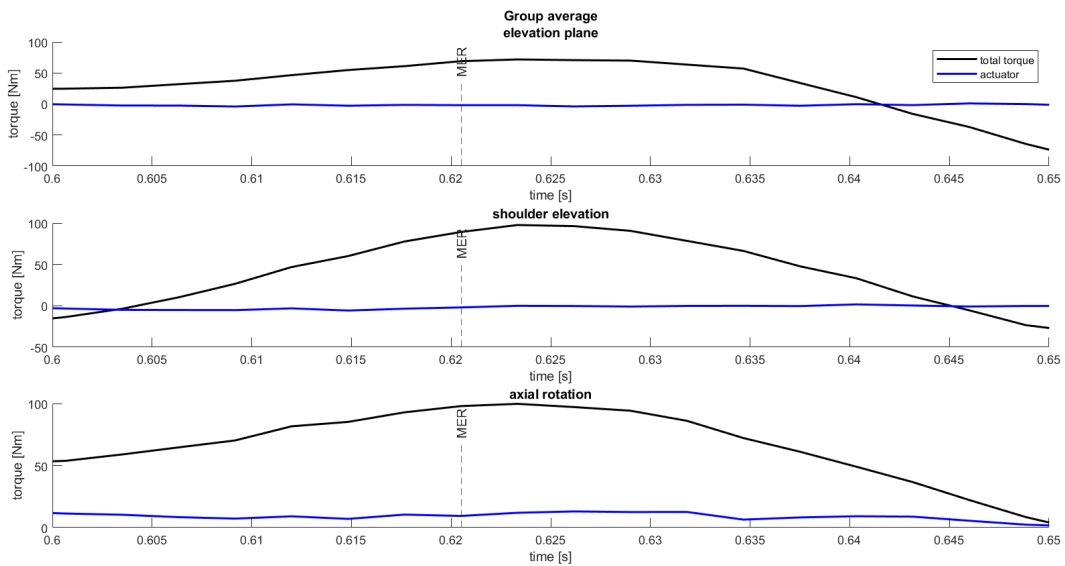


Figure 10: Torque produced by coordinate actuators during the pitching motion compared with total torque in the joint. Group average of all participants.

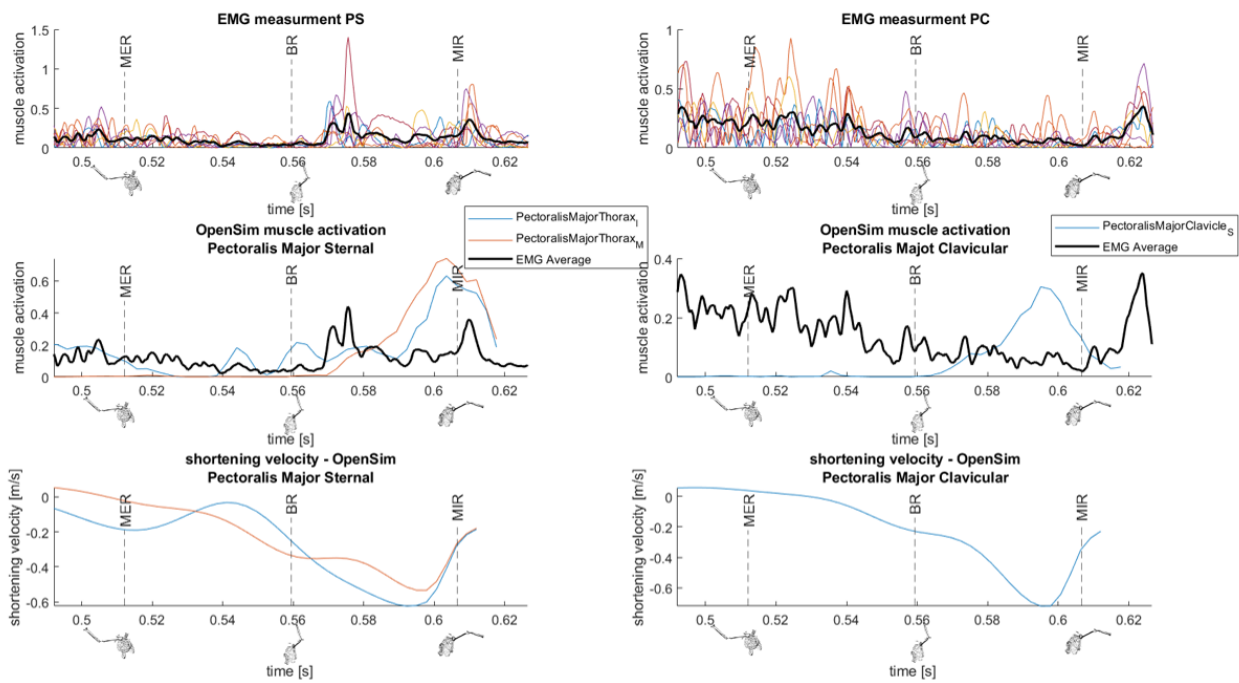


Figure 11: Data regarding pectoralis major of participant 1; From the top: measured EMG signal for 20 pitches, with average signal marked with a bold black line; muscle activation computed using OpenSim model and static optimization algorithm; muscle fibers' velocity based on the kinematics of the OpenSim model. PS - Pectoralis Major Sternal; PC - Pectoralis Major Clavicular

4 Discussion

The reason for performing the simulation was to find the correlation between the range of horizontal abduction of the subject and muscle activity, with the biggest emphasis on the pectoralis major and rotator cuff muscles. The initial data analysis has exposed discrepancies between resulted muscle activity and the expected one. Moreover, the muscle length in crucial moments of the pitching motion seemed to differ significantly from the one found in the literature. Furthermore, the computed activation of the coordinate actuators is too high for some participants, and the reason for its activity should be identified. For all mentioned reasons, it has been decided to first focus on a more detailed validation of the model.

4.1 Kinematic analysis

It was decided to start the model validation with an analysis of the angles between the thorax and humerus that are crucial for this study, namely horizontal abduction/adduction angle and axial rotation.

4.1.1 Horizontal abduction/adduction

The behavior of all participants is similar to the one described by Dillman, Fleisig, and Andrews [10]. Before reaching a point of MER, the arm with respect to the trunk is horizontally abducted (trunk rotates backward), and then between MER and BR, the trunk rotates forward first, and then the arm is horizontally adducted. The moment of this local minimum is shifted between participants, which can have two causes:

- difference in speed of the pitching - different duration of the acceleration phase (can be noticed in Figure 5);
- difference in pitching technique. Some pitchers may delay or speed up trunk forward rotation [18, 38].

The horizontal abduction measured by Hordijk [16] is as well similar to the one calculated using the OpenSim. One difference is the minimum after the MER, for Hordijk, the difference between the local minimum and preceding local maximum was smaller (like for participant 12 in the given experiment). However, that difference can be a result of the throwing technique and trunk movement described before.

4.1.2 Internal/External rotation

The angle of maximal external rotation varies between 139° and 177° . All participants performed dynamic shoulder internal rotation after MER. Though the range of movement can be different than one described by Dillman, Fleisig, and Andrews and Hordijk, the nature of the movement is similar. The differences in the range of axial rotation can have different backgrounds, such as differences in technique, to GRID (glenohumeral internal rotation deficit) [4, 29] or osseous adaptations of the glenohumeral joint (for example humeral torsion) [35]. For that reason, only the overall nature of the axial rotation has been evaluated.

4.1.3 Summary

To conclude, the movement of the humerus with respect to the thorax can be described as correct. However, there is uncertainty about the movement of the scapula. As described in section 2, there was only one marker on the scapula, and its movement was artificially limited to prevent flipping. Moreover, there is a big probability of omitting some dynamic movements of the scapula, as not enough information was delivered. For that reason, in further analysis, the biggest stress was put on the muscle not attached to the scapula, from the muscles of interest, is the pectoralis major. The rotator cuff muscles can be analyzed as well, but the uncertainty of the scapula kinematics has to be taken into account.

4.2 Muscle length

4.2.1 Pectoralis major

Pectoralis Major is expected to stay stretched and with a similar length during the acceleration phase [16]. Based on the data presented in the Figure 5, all three parts of pectoralis major stay stable during the acceleration phase for participants 3 and 12, as well as for participant 15 apart from the inferior thoracic part. However, only for participant 15, all three parts were stretched. It can be noticed that for all participants inferior thoracic part of the pectoralis major is barely stretched (with normalized muscle length not exceeding 1.1) or even contracted. There is no correlation between the level of the stretch of the pectoralis major and the range of the horizontal abduction of the pitchers during the acceleration phase.

Hordijk observed both clavicular and thoracic parts of pectoralis major to have a normalized length between

1.34 and 1.37 at the moment of MER [16]. In the presented research, only the clavicular part for participants 3 and 15 has a similar level of extension. To find the source of this discrepancy, the behavior of the pectoralis major was further investigated. As presented in section 3, the thoracic part of the pectoralis major remains contracted (or slightly stretched) for the entire range of movement in the horizontal abduction plane. Visual examination of the pectoralis major during the shoulder abduction was performed (Figure 12). The muscle is wrapping around the torso as expected and in range of the daily tasks (in which model was validated [32]). For the elevation plane angle of -5° , muscle position seems to be correct (Figure 12a), but for an angle of -10° muscle starts to go through the humeral head (Figure 12b). For an angle of -20° , the muscle goes entirely through humeral (Figure 12c). It is clear that wrapping around the humeral head and shaft was not ensured during model creation, and as a result, muscle is not sufficiently stretched. However, the wrapping problem does not explain the pectoralis major behavior entirely, as the unnatural behavior of the thoracic part of the pectoralis major can be observed for horizontal abduction smaller than 5° . One of the possible explanations is that the part of the muscle is too long. To check that possibility, the length of the thoracic part of the pectoralis major was shortened by 20% for every participant, and the normalized length of muscles was plotted against the angle of elevation plane (Figure 13). After shortening, the thoracic part of the pectoralis major is more extended. However, the muscle is still shorter than expected. The change of the muscle length by 20% is too big to be considered as the tuning of the model properties after scaling, and an even greater change is needed to ensure the correct behavior of the muscle, although further development of the scaling method of the muscles is needed. The current method uses the same scaling factors to scale muscle lengths as to scale bones. It is possible that there are some discrepancies in scaling the thorax width, which can cause errors in the pectoralis major length (as there is no problem with the clavicle part of the muscle).

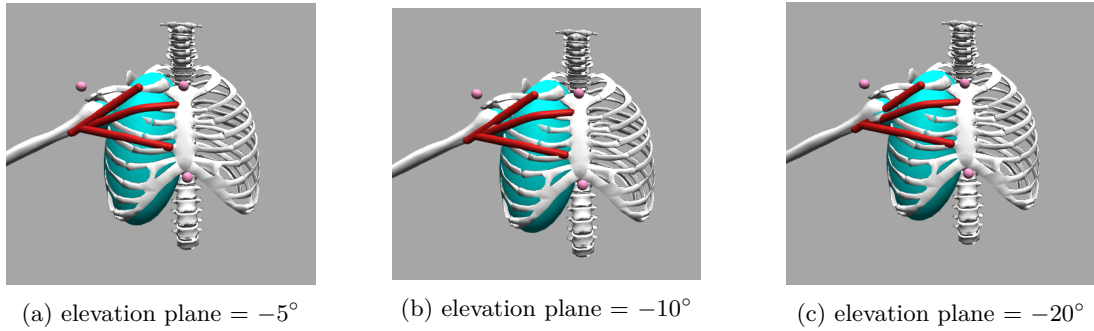


Figure 12: Position of the pectoralis major during the horizontal abduction of the arm. Shoulder elevation was set to 90° , axial rotation was set to 0° and the angle of the elevation plane (coordinate of the glenohumeral joint) was gradually changed.

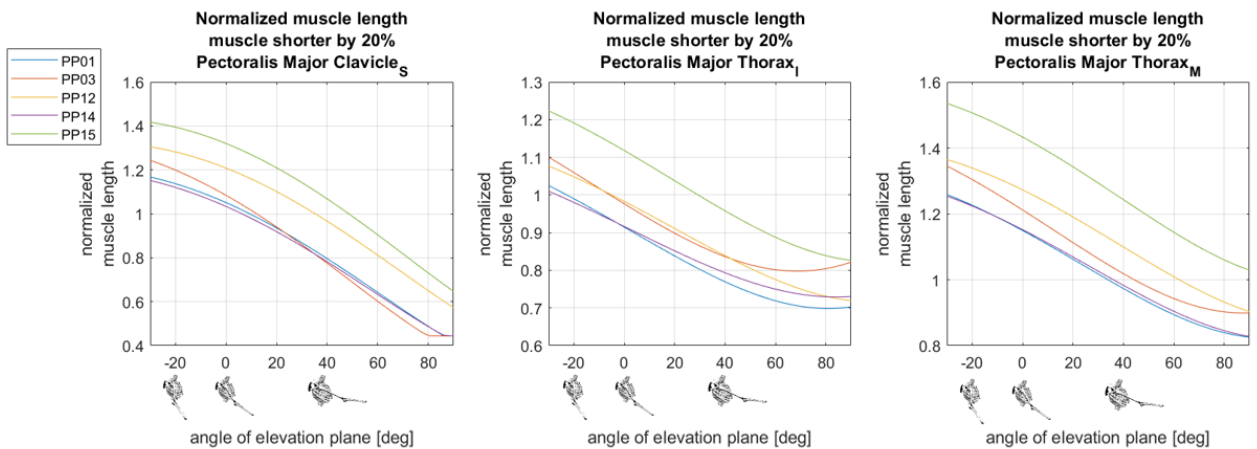


Figure 13: For the thoracic part of muscle shorten by 20%: normalized length (muscle length/optimal muscle length) of the pectoralis major with respect to the elevation plane coordinate of the glenohumeral joint. Comparison between participants. Shoulder elevation = 90° and axial rotation = 0° .

4.2.2 Rotator cuff

Even though there is a big uncertainty about scapula movement, the normalized length of the rotator cuff muscles was examined. According to the Hordijk [16], all rotator cuff muscles, apart from the teres major, should be contracted at the moment of MER. For measured data, both parts of supraspinatus are contracted at a similar level to the one examined by Hordijk. At the same time, the relative length of the infraspinatus deviates from the measurement from Hordijk. However, the relative length reported by Hordijk is extremely short, and the exact value may be a result of some error, the muscle should be contracted, which is not true for the results obtained from the OpenSim model. The subscapularis muscle, according to the Hordijk should have a normalized length of around 0.69, while for the measured data, it is around 1.1 (see Table 8). None of those values seems to be realistic, the muscle is supposed to be contracted. However, the value obtained by Hordijk seems to be too low. The only muscle stretched according to Hordijk is teres major, which is as well stretched for the measured data. Though, as with most of the aforementioned rotator cuff muscles, the relative length obtained from the OpenSim model is, on average higher than the one reported by Hordijk.

Apart from the length of muscles at a specific moment, it is helpful to compare the muscle length over time. While comparing the experimental results with data presented by Hordijk [16], more similarities could be found. For both models, the supraspinatus (Figure 18) and infraspinatus (Figure 17) are in local maximum for MER. It is not possible to see if muscles behave in a similar manner at BR and MIR moments, as Hordijk has indicated MER moment solely. The only evaluated muscle with visibly different behavior is teres major (Figure 19). Teres major in the model used in this paper is gradually stretched during the pitching motion when for Hordijk its behavior is more similar to one of infraspinatus and supraspinatus. It is worth noticing that the behavior of all evaluated muscles has similar nature for all participants. The only exception is the teres major of participant 15, which is visibly different.

4.2.3 Summary

It is impossible to draw any conclusions about the relation between maximal horizontal abduction and muscle behavior, as there is uncertainty regarding the validity of the results. The pectoralis major length is one of the most significant uncertainties. It was concluded that the thoracic part of the muscle is probably too long. Moreover, problems with a wrapping of the pectoralis major around the humeral head were as well identified. The discrepancies in the length of the pectoralis major are most probably caused by errors in the model scaling method. For that reason, it cannot be ruled out that there are errors in the scaling of all other muscles. However, the lengths of the rotator cuff muscles, apart from teres major, are similar to one found in the literature.

4.3 Muscle activation

Before the static optimization maximum forces of the model were scaled, the scaling factor was the same for all participants and was equal to 10. The resultant maximal isometric forces seem to be too high (see Table 9). However, the model was not able to perform pitching motion for a lower scaling factor. Even with the high isometric forces, the model of participant 12 reaches maximal activation for some muscles (see subsection B.4.1). Hordijk [16] also scaled the maximal force of the model. He based the scaling factor on the experimental data of subjects performing force tasks in six directions, the resulting scaling factors were not higher than 2.02.

There are two reasons why the model used in described research needs to be stronger than expected:

- the static optimization algorithm does not use an approximation of the movement between the steps. As a result, the accelerations are higher than the real ones. That theory is partially an answer, as upsampling data to 360Hz has lowered the needed scaling factor. While data of frequency of 120Hz were used, the needed scaling factor was between 50 and 100. However, no big difference in muscle activation was detected while data were upsampled to a frequency of 480Hz;
- muscles are not modeled correctly. If in a given position, muscles are not as stretched or as contracted as they should be from a physiological point of view, then they probably are not fulfilling their tasks correctly. In the used model, the pectoralis major is not stretched enough during the acceleration phase, which may result in its different activity and not producing the expected force and torque. In that case, other muscles would be forced to compensate for the pectoralis major (which should be one of the main contributors Escamilla and Andrews, Mlynarek, Lee, and Bedi), which leads to weaker muscles needing to be stronger than that would be in real life.

However, increasing the scaling factor and, thereby, maximal isometric forces would not influence the correctness of the static optimization results. Forces and torques would be higher than expected, but the moments of the

activation of the muscles should be correct. For that reason, discrepancies in muscle behavior are probably the result of the latter described reason, errors in the modeling of the muscles.

4.3.1 Torque

Static optimization is computing muscle activity partially determined by the torque required to fulfill acceleration in the joints [1]. Torque, calculated based on the static optimization results, takes into account not only muscle activation but also muscle properties (such as muscle force-length relation) and muscle geometry (moment arm). For that reason, it was decided to focus mostly on the produced torque while analyzing the results of static optimization.

Taking into consideration dynamic internal rotation movement during the acceleration phase, "the glenohumeral internal rotators (subscapularis, pectoralis major and latissimus dorsi)" [11] are expected to contribute significantly to the acceleration motion. Mlynarek, Lee, and Bedi [27] also suggested a high activity of pectoralis major, latissimus dorsi, and serratus anterior during the acceleration phase.

For the modeled pitching motion, the subscapularis is the muscle with the biggest contribution in internal/external rotation for all participants, but for participant 1. Escamilla and Andrews [11] suggested that very high activity of the subscapularis results from muscle function, of the steering humeral head to maintain in the glenoid. The next muscles with the biggest contribution during the acceleration phase in the external/internal rotation plane are the infraspinatus and supraspinatus, which is in accordance with the results of Escamilla and Andrews [11]. The high or moderate activity of rotator cuff muscles is as expected. Although, high activity of the pectoralis major was not detected. In fact, the pectoralis major is only 5th most contributing muscle to torque at MER, and 9th at BR.

Surprisingly, the muscle with the highest contribution during the acceleration phase is deltoideus (it has the biggest contribution for both X and Y components of the torque). Escamilla and Andrews reported moderate deltoideus activity during the acceleration phase, while Mlynarek, Lee, and Bedi did not mention it.

While discussing the torque produced by the muscles is crucial to check if the torque produced by coordinate actuators is close to zero, which is not the case for most of the participants. In fact, only for participant 3, the contribution of the coordinate actuators is close to zero for all degrees of freedom of the glenohumeral joint. For most of the participants, the coordinate actuators are the most active on the axial rotation plane, which indicates that shoulder internal and external rotators are not acting as expected.

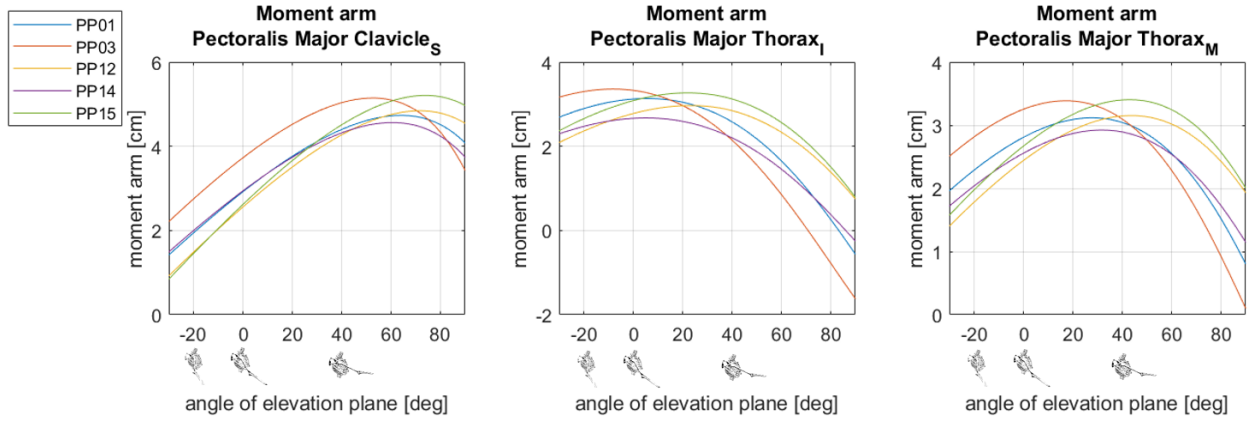
To provide more insight into pectoralis major behavior, its moment arm was analyzed. The results for the moment arm used for *elevation plane* torque and for *axial rotation* torque are presented in Figure 14. The data regarding shoulder elevation are included in Appendix B. Based on the Figure 14a, it can be noticed that the thoracic inferior part of the muscle is the only one with a greater moment arm when the shoulder is horizontally abducted than for horizontal adduction. The reason for that can be that only this part of the pectoralis major does not intersect with the humeral head during the horizontal abduction (Figure 12c). The moment arm in the axial rotation plane was expected to be low, and for any of the participants, it is not higher than 1cm in the evaluated range of motion.

4.3.2 Comparison between participants

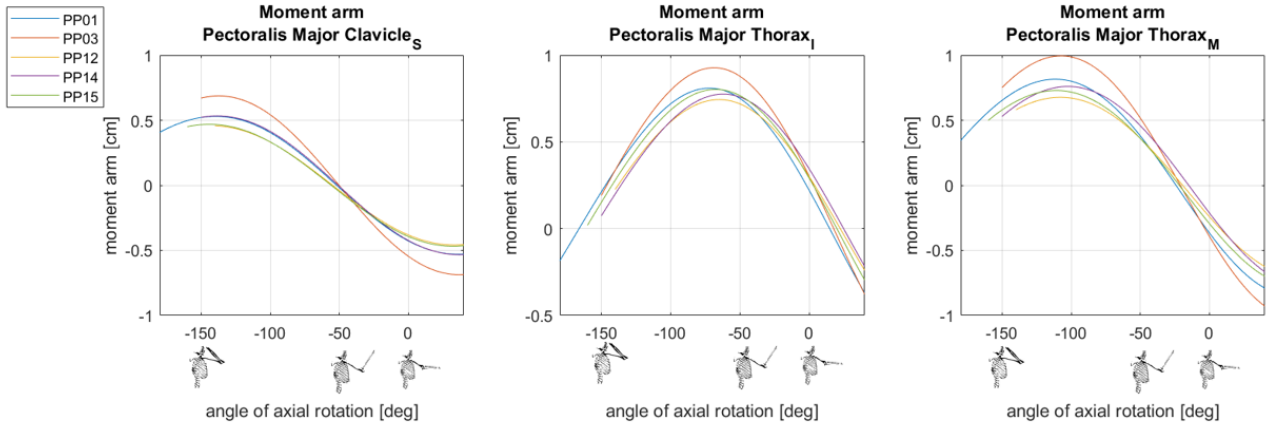
Based on the presented results, it was decided that participant's 3 behavior is the most correct. All parts of the pectoralis major are stretched during the acceleration phase, and the pectoralis major is among the most active muscles at moments of the MER and BR. Additionally, the contribution of the coordinate actuators is lowest for participant 3. On the other hand, participant 15 was deemed to yield the least realistic results, with the contribution of the coordinate actuators being the highest in both MER and BR moments. Moreover, at the moment of BR, the coordinate actuator has the second highest contribution in axial rotation torque.

The comparison of the two allows gaining insight into the probable causes of the discrepancies between results obtained based on the OpenSim simulations and the expected ones. First of all, it is worth comparing the range of motion of the participants. The difference in range of the external rotation is equal to about 5° , which does not seem to be a big difference, as the value is close to 150° for both of the participants and was changed from 90° in the original Thoracoscapular Shoulder Model. However, the changed range of axial rotation may contribute to problems with the wrapping of the muscles around the humeral shaft. The difference in the horizontal abduction of the arm at the moment of MER seems to be more significant. The arm of the PP03 stays horizontally adducted (10.68°), while PP15 horizontally abducts the arm (the angle of horizontal adduction is equal to -16.42°). That difference can influence the correctness of the results and how significant the lack of wrapping around the humeral head is (see Figure 12).

Additionally, no visible differences between the moment arm of the pectoralis major were found between models



(a) Moment arm of pectoralis major for elevation plane, measured at 90° of shoulder elevation angle



(b) Moment arm of pectoralis major for axial rotation, measured at 90° of shoulder elevation angle and elevation plane angle of 0° .

Figure 14: Moment arm of pectoralis major for (a) *elevation plane* and (b) *axial rotation*

for axial rotation (Figure 14b), while the visible shift between curves corresponding to PP03 and PP15 is visible for elevation plane (Figure 14a). Moreover, the participant with the most similar moment arm of pectoralis major with respect to the elevation plane to the PP15 is the PP12. The contribution of the coordinate actuators for PP12 was the second highest after PP15. Having that in mind, it can be said that the correctness of the moment arm of the muscles should be ensured before the simulation.

4.3.3 EMG data

Because only one component of the acceleration was saved during the data acquisition, there are some uncertainties about the correctness of the synchronization. The lack of measured activity of the pectoralis major during the acceleration phase is itself the source of uncertainty about the correctness of the data synchronization. Escamilla and Andrews [11] and Mlynarek, Lee, and Bedi [27] have measured the activity of the muscles and reported high activity of pectoralis major during the acceleration phase. It was decided not to proceed with data validation with the EMG signal.

4.3.4 Summary

The faulty geometry of the pectoralis major is, most probably, the source of the errors in the static optimization results. For that reason, no conclusions regarding the research question can be derived from the results. However, the activity of the rotator cuff muscles was in accordance with the results from the literature [11, 27]. Presumably, fixing the scaling of the pectoralis major and its wrapping around the humeral head could solve the errors and enable obtaining the correct results from the static optimization. It is possible that even for

the adjusted model the scaling factor will remain high, yet for the reasons mentioned at the beginning of the [subsection 4.3](#), the timing of the muscle activity should stay correct.

4.4 Recommendations

The main recommendation is to repeat the research and data collection. With the correct model and sufficient data, it should be possible to answer the question, *How does the range of horizontal abduction influence the activity of the muscles?*, using the methodology proposed in this paper. The recommendations about what should be improved before repeating the research can be divided into three categories: motion data collection, model development, and EMG data collection. More detailed recommendations are presented below.

4.4.1 Motion data collection

First, data used in this research were not gathered to be used with musculoskeletal models, as a consequence, the static motion of not all participants was recorded with all markers visible. That fact cuts the number of participants by almost half, which limits the statistical significance of the potential results. It is recommended to ensure that static pose is well recorded (with all markers visible) while gathering data to replicate this study. Without all markers visible during the static phase, it is impossible to calculate scaling factors of body segments with sufficient accuracy and consequently scale the model correctly.

The number of participants was also limited by the fact that the used model was right-handed, which excluded all subjects with the left dominant upper limbs. To solve this, the motion data of the pitchers with a dominant left hand can be mirrored and used with the existing model.

However, the most crucial improvement for motion data collection is to record the scapula position during pitching. In the current data set, only one marker was situated on the scapula, which makes it impossible to not only model the motion of the scapula correctly but also to scale it properly (the scapula needed to be scaled with the use of the no-scapular markers - see [Table 7](#)). It can be difficult to record the scapula motion accurately, and with such dynamic motion as a baseball pitch, there will be uncertainty about marker location with respect to the actual bone. Although, a simulation based on the data will be more trustworthy than one based on one marker and constraints regarding the possible movement of the scapula.

It is necessary to model scapular movement correctly to answer the research question fully. Not only will the muscles' position and length be influenced, but also the orientation of the scapula itself can provide useful insight into player technique. Some authors are pointing the scapular movement as one of the main reasons for the occurrence of the hyperangulation and, consequently, excessive horizontal abduction [[4](#), [19](#), [21](#), [25](#)].

The scapular motion should be tracked with the use of 3 markers, to fully determine the position and orientation of the bone, it is suggested to place the markers based on the Seth et al. [[31](#)].

4.4.2 Model development

The non-physiological behavior of the pectoralis major is described and visualized before (see [Figure 12](#)). The geometry of all muscles of the model was evaluated in the position of excessive horizontal abduction and external rotation. Below are presented muscles that may not wrap correctly around the larger humeral head or/and shaft of the humerus:

- Coracobrachialis
- Latissimus Dorsi (for external rotation greater than 100°)
- Pectoralis Major
- Teres Major (for external rotation greater than 100°)
- Biceps (BIC_brevis part)

It was indicated that Supraspinatus does not wrap around the scapula for external rotation greater than 100° in a position of horizontal abduction.

To solve the problems with wrapping, muscle geometry should be modified. The modification can be done in two ways: in the source code of the model (changes in *PathWrapSet* in model definition) or by modifying the model in OpenSim Creator (<https://opensimcreator.com/>). The latter option is recommended, as it enables the preview of muscle properties while adjusting the model. The geometry path of the aforementioned muscles should be modified by adding needed wrapping (around the humeral head for most of the muscles). It is crucial to ensure that implemented changes do not influence the moment arm of the muscle in a validated range of motion. Additionally, the moment arm for an increased range of horizontal abduction and external rotation

should be validated. Some researchers have performed experiments to specify the moment arm of the muscles connected to the glenohumeral joint [15, 22, 23], yet there is a possibility that it can be challenging to find sources indicating the moment arm of muscles in the entire range of movement of baseball pitchers.

The second non-physiological characteristic of the pectoralis major is the length of its thorax part, muscle seems to be too long. Probably, muscle length has been scaled incorrectly during the geometric scaling. The methodology of scaling the pectoralis major should be evaluated with details. Taking into consideration that only the thoracic part of the muscle seems to be too long, it is possible that the thoracic and clavicular parts of the muscle have been scaled separately. In used optimization algorithm, the muscle length is scaled together with bones, it is thought possible that the clavicular part of the pectoralis major has been scaled with the clavicle and the thoracic part with the thorax (probably the width of the thorax). If that is true, all other muscles scaled with the same factor as the thorax should be evaluated, they can also be too long, and consequently, they do not contribute to the motion in the way they should. Moreover, it can also be ensured that the entire muscle is scaled with the same factor, even if parts of it are attached to different bone segments.

4.4.3 EMG data collection

Finally, the surface EMG measurement can be used to validate results from the OpenSim model, to do so, EMG data need to be synchronized with the kinematic results. The alignment based on the accelerometer data may be the easiest option, though all components of the thorax acceleration should be recorded. The use of the total acceleration, not only one component, would eliminate errors connected with slight differences in coordinate system definitions and make data synchronization easier. Additionally, the placement of the marker close to the accelerometer can be beneficial. The marker does not need to be used to perform inverse kinematics, but its position will simplify the calculation of the acceleration from the model and increase the quality of data alignment.

5 Conclusion

The methodology used in this study is believed to be correct, and with improvements presented in the [subsection 4.4](#), it should be possible to answer the research question. Based on the kinematic data, the differences between the range of horizontal abduction/adduction between pitchers can be identified. One of the examined pitchers does not horizontally abduct the arm at the time of MER, while the rest of the participants perform horizontal abduction between 0° and 20° . The horizontal abduction/adduction is also the only angle describing orientation between the thorax and humeral, for which the significant differences in nature of the movement (different than the range of motion) are visible. For that reason, it is concluded that based on the gathered data, it should be possible to detect if there are differences in the pectoralis major activity correlated to the angle of horizontal abduction/adduction. There is significant uncertainty regarding the movement of the scapula, as there was only one marker placed on that bone during the data recording. For that reason, it is important to take that uncertainty into account while analyzing the rotator cuff muscles. change about muscle length, add scapula movement, and that rotator cuff muscles seem to be correct.

The muscle length was derived from the kinematic data. To simplify the statistical analysis, muscle length has been divided by the optimal muscle length. Normalized muscle length greater than 1 indicates stretched muscles, and lower than 1 indicates contracted muscles. The normalized length of all rotator cuff muscles, but teres major, was similar to the one described by Hordijk [16]. There were discrepancies found between the simulated muscle's length of the pectoralis major and the ones found in the literature. Only the clavicular part of the pectoralis major could be described as stretched at the expected level. Moreover, parts of the thoracic part of the pectoralis major were slightly stretched (below 1.1) or even contracted. From an analysis of the pectoralis major optimal length plotted against elevation plane coordinate, it could be noticed that the length of the muscle is not increasing enough during the arm abduction. It was concluded that the thoracic parts of the pectoralis major seem to be too long. The length of the muscle was once again evaluated against the elevation plane after shortening the thoracic part of the pectoralis major by 20%. The inferior thoracic part of the muscle stayed stretched below 1.1 for most of the participants at the elevation plane angle of -20° , but improvement in the results could be noticed. It was concluded that part of the muscle was incorrectly scaled. The further visual examination has shown that the pectoralis major muscle is not wrapping correctly around the humeral for horizontal abduction of the arm.

Based on that information, it was concluded that the static optimization algorithm will not compute the correct muscle activity, as one of the most crucial muscles during the acceleration phase is not modeled correctly for the entire range of motion of baseball pitchers. Nevertheless, based on the computed activation of the muscles, the

torque produced by them has been calculated. The contribution of the rotator cuff muscles in the abduction and horizontal abduction planes was significant and consistent with the literature. However, pectoralis major has a smaller contribution than described in the literature, and deltoideus' muscle activation was high, while it was described as moderate by Escamilla and Andrews [11]. Additionally, the joint actuators were active, which indicates that not all muscles have fulfilled their role. The conclusion was drawn that error with the pectoralis major behavior has influenced most of the results of the static optimization, and other muscles have compensated for the pectoralis major. The compensation for the action, normally performed by pectoralis major, has influenced the required maximal isometric force of the model's muscles to be able to perform a given task. For that reason, the forces and torques produced by the model are unnaturally high. While solving modeling problems, one should be able to lower the scaling factor of the maximal forces of the model and, as a result, obtain physiological values from the final analysis.

Finally, several improvements to model development and experimental data acquisition are proposed. First, the error with scaling of the pectoralis major thoracic head needs to be addressed. Presumably, the thoracic part of the pectoralis major was scaled with the same scaling factor as the thorax. If that is the reason for the problem with the muscle length, the scaling of all muscles attached to the thorax should be evaluated. Next, it is suggested to fix wrapping problems of the glenohumeral muscles. Apart from pectoralis major, coracobrachialis, latissimus dorsi, teres major, supraspinatus, and biceps (BIC_brevis part) were identified to have non-physiological behavior around the humeral head, in positions of excessive horizontal abduction and external rotation. Solving problems with scaling and wrapping of the muscles should allow conducting analysis on all muscles not contacted with the scapular bone while using the current data set. Moreover, improvements in motion data collection are suggested. The most significant recommendation is the placement of more markers on the scapula to track this bone movement better. That change would enable simulating the movement of the scapula with greater reliability and consequently allow analysis based on the rotator cuff muscles.

It is believed that after the implementation of the proposed recommendations, it should be possible to study the relationship between a range of horizontal abduction and muscle activity while using the steps and methodology described in the given paper. Unfortunately, the described problems made it impossible to draw any conclusions, regarding the research question, from the obtained results.

5.1 Recommended improvement in OpenSim and Thoracoscapular Shoulder Model

- Ensuring correct muscle paths in the Thoracoscapular Shoulder Model;
- Clearer information about the scaling of the muscles and their properties;
- Access to the plots representing properties of the muscle (e.g., force-length relationship), not only to the parameters of the plot. It would make analysis more intuitive;
- "Beginners guide" for the OpenSim, including guidelines on how to check the validity of the model after making modifications.

References

- [1] Italo Belli. *PTbot repository*. Version 0.1.0. Nov. 2022. URL: <https://github.com/ComputationalBiomechanicsLab/PTbot>.
- [2] Sepp Braun, Dirk Kokmeyer, and Peter J Millett. “Shoulder injuries in the throwing athlete”. In: *JBJS* 91.4 (2009), pp. 966–978. ISSN: 0021-9355.
- [3] Mary D. Klein Breteler, Cornelis W. Spoor, and Frans C.T. Van der Helm. “Measuring muscle and joint geometry parameters of a shoulder for modeling purposes”. In: *Journal of Biomechanics* 32.11 (1999), pp. 1191–1197. ISSN: 0021-9290.
- [4] Stephen S Burkhart, Craig D Morgan, and W Ben Kibler. “The disabled throwing shoulder: spectrum of pathology Part I: pathoanatomy and biomechanics”. In: *Arthroscopy: The Journal of Arthroscopic & Related Surgery* 19.4 (2003), pp. 404–420. ISSN: 0749-8063.
- [5] Gary J Calabrese. “Pitching mechanics, revisited”. In: *International journal of sports physical therapy* 8.5 (2013), p. 652.
- [6] Samuel K. Chu et al. “The Kinetic Chain Revisited: New Concepts on Throwing Mechanics and Injury”. In: *PM&R* 8.3S (2016), S69–S77. ISSN: 1934-1482.
- [7] Keith T. Corpus et al. “Evaluation and treatment of internal impingement of the shoulder in overhead athletes”. In: *World Journal of Orthopedics* 7.12 (2016), p. 776. ISSN: 2218-5836.
- [8] JT Davis et al. “The effect of pitching biomechanics on the upper extremity in youth and adolescent baseball pitchers”. In: *The American journal of sports medicine* 37.8 (2009), pp. 1484–1491. ISSN: 0363-5465.
- [9] Scott Delp et al. “OpenSim: Open-Source Software to Create and Analyze Dynamic Simulations of Movement”. In: *Biomedical Engineering, IEEE Transactions on* 54 (Dec. 2007), pp. 1940–1950.
- [10] Charles J. Dillman, Glenn S. Fleisig, and James R. Andrews. “Biomechanics of Pitching With Emphasis Upon Shoulder Kinematics”. In: *Journal of Orthopaedic & Sports Physical Therapy* 18.2 (), pp. 402–408. ISSN: 0190-6011.
- [11] Rafael F. Escamilla and James R. Andrews. “Shoulder Muscle Recruitment Patterns and Related Biomechanics during Upper Extremity Sports”. In: *Sports Medicine* 39.7 (2009), pp. 569–590. ISSN: 0112-1642.
- [12] Glenn S. Fleisig et al. “Kinematic and Kinetic Comparison between Baseball Pitching and Football Passing”. In: *Journal of Applied Biomechanics* 12.2 (1996), pp. 207–224. ISSN: 1065-8483.
- [13] Hermie J Hermens et al. “European recommendations for surface electromyography”. In: *Roessingh research and development* 8.2 (1999), pp. 13–54.
- [14] Benton E Heyworth and Riley J Williams. “Internal impingement of the shoulder”. In: *The American Journal of Sports Medicine* 37.5 (2009), pp. 1024–1037. ISSN: 0363-5465.
- [15] Freya Hik and David C. Ackland. “The moment arms of the muscles spanning the glenohumeral joint: a systematic review”. In: *Journal of Anatomy* 234.1 (2019), pp. 1–15. ISSN: 0021-8782.
- [16] Peter Hordijk. “Musculoskeletal modelling of the shoulder during baseball pitching”. Unpublished MSc thesis. 2017.
- [17] Christopher M Jobe. “Posterior superior glenoid impingement: expanded spectrum”. In: *Arthroscopy: The Journal of Arthroscopic & Related Surgery* 11.5 (1995), pp. 530–536. ISSN: 0749-8063.
- [18] David W. Keeley et al. “A Biomechanical Analysis of Youth Pitching Mechanics”. In: *Journal of Pediatric Orthopaedics* 28.4 (2008). ISSN: 0271-6798.
- [19] W. Ben Kibler, Trevor Wilkes, and Aaron Sciascia. “Mechanics and Pathomechanics in the Overhead Athlete”. In: *Clinics in Sports Medicine* 32.4 (2013), pp. 637–651. ISSN: 0278-5919.
- [20] Chlodwig Kirchoff and Andreas B Imhoff. “Posterosuperior and anterosuperior impingement of the shoulder in overhead athletes: evolving concepts”. In: *International orthopaedics* 34.7 (2010), pp. 1049–1058. ISSN: 1432-5195.
- [21] Michael Knesek et al. “Diagnosis and management of superior labral anterior posterior tears in throwing athletes”. In: *The American journal of sports medicine* 41.2 (2013), pp. 444–460. ISSN: 0363-5465.
- [22] David K. Kuechle et al. “Shoulder muscle moment arms during horizontal flexion and elevation”. In: *Journal of Shoulder and Elbow Surgery* 6.5 (1997), pp. 429–439. ISSN: 1058-2746.

- [23] David K. Kuechle et al. “The relevance of the moment arm of shoulder muscles with respect to axial rotation of the glenohumeral joint in four positions”. In: *Clinical Biomechanics* 15.5 (2000), pp. 322–329. ISSN: 0268-0033.
- [24] Dana J Lin, Tony T Wong, and Jonathan K Kazam. “Shoulder injuries in the overhead-throwing athlete: epidemiology, mechanisms of injury, and imaging findings”. In: *Radiology* 286.2 (2018), pp. 370–387. ISSN: 0033-8419.
- [25] Teruhisa Mihata et al. “Excessive glenohumeral horizontal abduction as occurs during the late cocking phase of the throwing motion can be critical for internal impingement”. In: *The American journal of sports medicine* 38.2 (2010), pp. 369–374. ISSN: 0363-5465.
- [26] M. Millard et al. “Flexing computational muscle: modeling and simulation of musculotendon dynamics”. In: *J Biomech Eng* 135.2 (2013), p. 021005. ISSN: 0148-0731 (Print) 0148-0731.
- [27] Ryan A Mlynarek, Simon Lee, and Asheesh Bedi. “Shoulder injuries in the overhead throwing athlete”. In: *Hand clinics* 33.1 (2017), pp. 19–34. ISSN: 0749-0712.
- [28] Hugue Ouellette et al. “Spectrum of shoulder injuries in the baseball pitcher”. In: *Skeletal Radiology* 37.6 (2008), pp. 491–498. ISSN: 0364-2348.
- [29] Michael M. Reinold et al. “Internal Impingement”. In: *The Athlete’s Shoulder*. Second. Churchill Livingstone Elsevier, 2009. Chap. 11, pp. 123–141.
- [30] Ajay Seth and Matt Millard. *OpenSim::Muscle Class Reference*. Aug. 2022. URL: https://simtk.org/api_docs/opensim/api_docs/classOpenSim_1_1Muscle.html#details.
- [31] Ajay Seth et al. “A Biomechanical Model of the Scapulothoracic Joint to Accurately Capture Scapular Kinematics during Shoulder Movements”. In: *PLOS ONE* 11.1 (2016), e0141028. ISSN: 1932-6203.
- [32] Ajay Seth et al. “Muscle Contributions to Upper-Extremity Movement and Work From a Musculoskeletal Model of the Human Shoulder”. In: *Frontiers in Neurorobotics* 13 (2019). ISSN: 1662-5218.
- [33] Ajay Seth et al. “OpenSim: Simulating musculoskeletal dynamics and neuromuscular control to study human and animal movement”. In: *PLOS Computational Biology* 14.7 (2018), e1006223. ISSN: 1553-7358.
- [34] Ulrich J Spiegl, Ryan J Warth, and Peter J Millett. “Symptomatic internal impingement of the shoulder in overhead athletes”. In: *Sports medicine and arthroscopy review* 22.2 (2014), pp. 120–129. ISSN: 1062-8592.
- [35] B. A. Sweitzer et al. “A comparison of glenoid morphology and glenohumeral range of motion between professional baseball pitchers with and without a history of SLAP repair”. In: *Arthroscopy* 28.9 (2012), pp. 1206–13. ISSN: 1526-3231 (Electronic) 0749-8063 (Linking).
- [36] Mike Urbin et al. “Associations Between Timing in the Baseball Pitch and Shoulder Kinetics, Elbow Kinetics, and Ball Speed”. In: *The American journal of sports medicine* 41 (2012). DOI: [10.1177/0363546512467952](https://doi.org/10.1177/0363546512467952).
- [37] H Van der Hoeven and W Ben Kibler. “Shoulder injuries in tennis players”. In: *British journal of sports medicine* 40.5 (2006), pp. 435–440. ISSN: 0306-3674.
- [38] Jason L Zaremski, Giorgio Zeppieri, and Brady L Tripp. “Injury prevention considerations in adolescent overhead-throwing athletes”. In: *Current Physical Medicine and Rehabilitation Reports* 7.3 (2019), pp. 216–226. ISSN: 2167-4833.

A Markers placement

The placement of markers is presented in the [Figure 15](#) and explained in [Table 6](#).

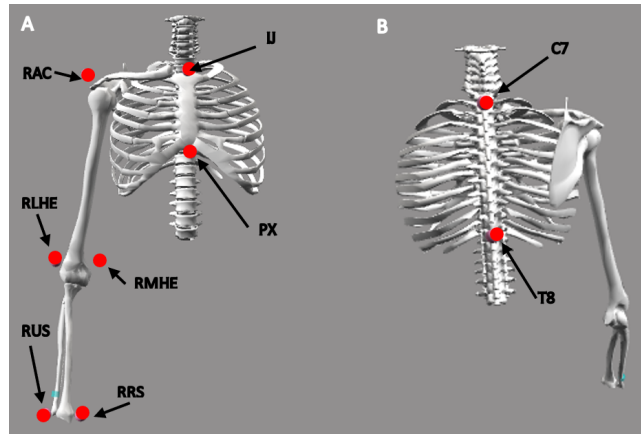


Figure 15: Position of the markers presented on the Thoracoscapular model in OpenSim environment. A: anterior view; B: posterior view; Explanation of the names of the markers is presented in [Table 6](#)

Table 6: Explanation of the markers names presented in the [Figure 15](#)

Marker	Marker location	Reference body segment
IJ	Incisura jugularis	Thorax
PX	Xyphoid process	Thorax
C7	7th cervical vertebra	Thorax
T8	10th thoracic vertebra	Thorax
RAC	Acromion	Scapula
RLHE	Lateral epicondyle of the humerus	Humerus
RMHE	Medial epicondyle of the humerus	Humerus
RUS	Ulnar styloid process	Ulna
RRS	Radial styloid process	Radius

B OpenSim analyses

B.1 Model scaling

The relations used to create scaling ratios for body segments are presented in [Table 7](#).

Table 7: Relations used to create scaling ratios

body segment	direction	marker 1	marker 2
Thorax	X	IJ	C7
		T8	PC
	Y	IJ	PX
		C7	T8
	Z	IJ	PX
		C7	T8
IJ		C7	
T8		PX	
Clavicle	X Y Z	IJ	PX
		C7	T8
		IJ	C7
		T8	PX
Scapula	X Y Z	RAC	RMHE
		RAC	RLHE
		IJ	PX
		C7	T8
		IJ	C7
Humerus	X Y Z	RAC	RMHE
		RAC	RLHE
Radius Ulna	X Y Z	RUS	RMHE
		RRS	RLHE

B.2 Muscle length

[Figure 16](#) – [Figure 19](#) present normalized muscle length during the pitching motion, for all muscles of interest.

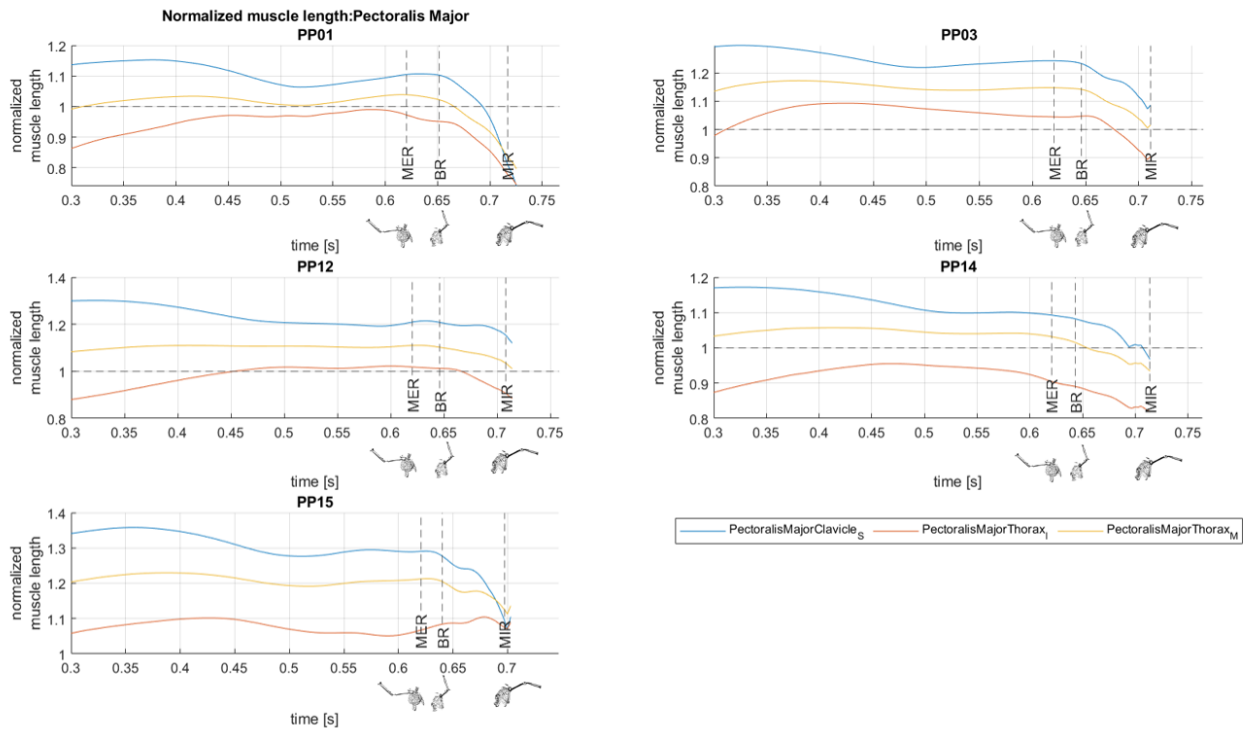


Figure 16: Pectoralis Major - normalized muscle length during the pitching motion.

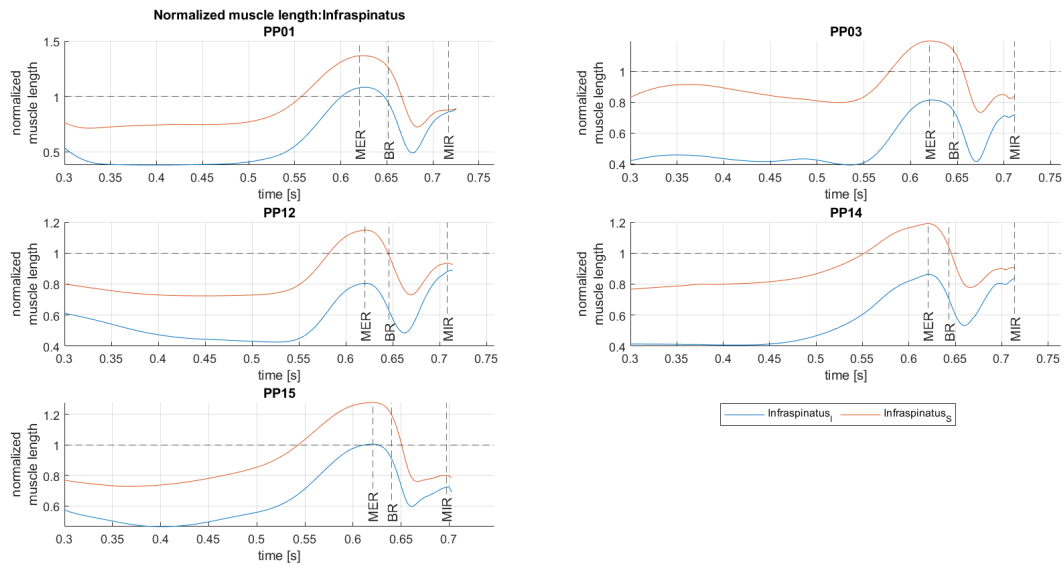


Figure 17: Infrasinatus - normalized muscle length during the pitching motion.

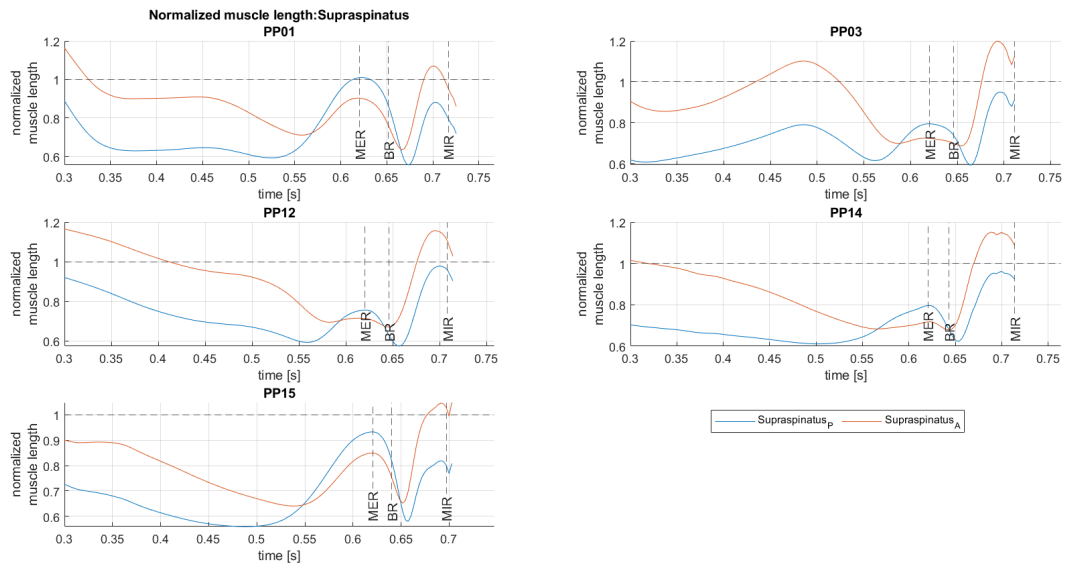


Figure 18: Supraspinatus - normalized muscle length during the pitching motion.

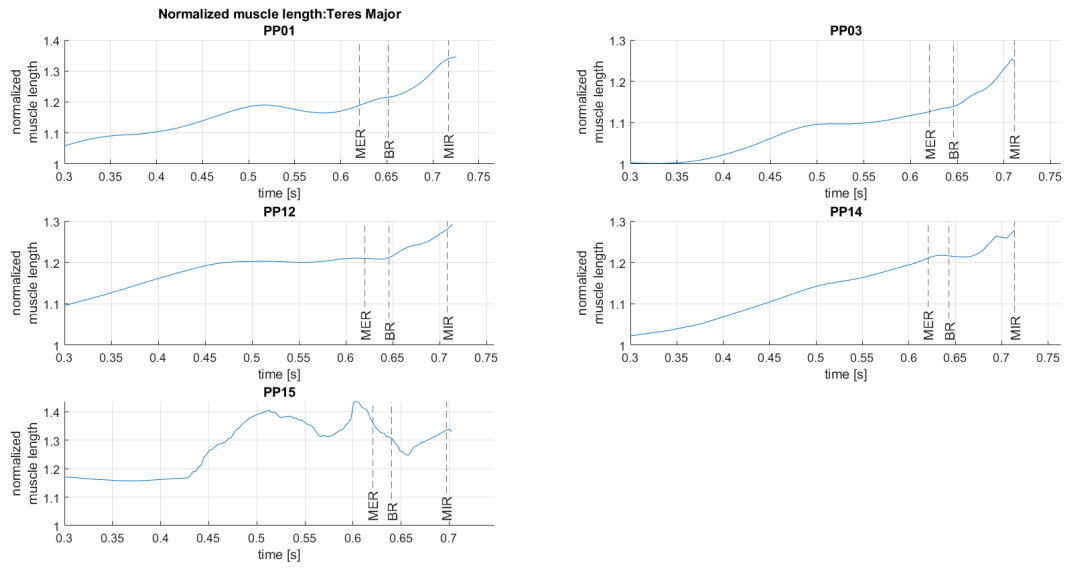


Figure 19: Teres Major - normalized muscle length during the pitching motion.

Muscle length at the moment of MER has been compared with results from Hordijk [16] (Table 8).

Table 8: Relative muscle length (muscle length/optimal muscle length) at moment of MER compared with results from Hordijk [16].

Muscle name	muscle length / optimal muscle length					Hordijk [16]
	PP01	PP03	PP12	PP14	PP15	
SerratusAnterior_I	1.227 ± 0.004	1.182 ± 0.004	1.095 ± 0.006	1.084 ± 0.029	1.211 ± 0.002	1.40 ± 0.12
SerratusAnterior_M	1.137 ± 0.004	1.099 ± 0.003	1.016 ± 0.004	1.049 ± 0.009	1.107 ± 0.004	
SerratusAnterior_S	0.939 ± 0.003	0.919 ± 0.003	0.692 ± 0.003	0.863 ± 0.008	0.683 ± 0.005	
PectoralisMajorClavicle_S	1.105 ± 0.004	1.243 ± 0.004	1.209 ± 0.004	1.093 ± 0.006	1.29 ± 0.004	1.34 ± 0.01
PectoralisMajorThorax_I	0.972 ± 0.003	1.044 ± 0.002	1.018 ± 0.001	0.905 ± 0.01	1.067 ± 0.008	1.37 ± 0.02
PectoralisMajorThorax_M	1.039 ± 0.001	1.148 ± 0.002	1.11 ± 0.002	1.032 ± 0.005	1.212 ± 0.004	
TeresMajor	1.189 ± 0.003	1.127 ± 0.007	1.21 ± 0.003	1.211 ± 0.009	1.362 ± 0.039	1.18 ± 0.04
Infraspinatus_I	1.079 ± 0.011	0.813 ± 0.008	0.805 ± 0.007	0.862 ± 0.035	1.005 ± 0.011	0.44 ± 0.05
Infraspinatus_S	1.366 ± 0.008	1.195 ± 0.006	1.148 ± 0.005	1.19 ± 0.027	1.277 ± 0.009	
Supraspinatus_P	1.01 ± 0.011	0.794 ± 0.006	0.756 ± 0.004	0.796 ± 0.029	0.933 ± 0.011	0.76 ± 0.04
Supraspinatus_A	0.903 ± 0.012	0.724 ± 0.004	0.713 ± 0.003	0.718 ± 0.021	0.85 ± 0.01	
DeltoideusClavicle_A	0.879 ± 0.006	1.033 ± 0.009	0.992 ± 0.007	0.878 ± 0.015	0.932 ± 0.007	1.00 ± 0.04
DeltoideusScapula_P	0.553 ± 0.006	0.427 ± 0.01	0.537 ± 0.005	0.614 ± 0.021	0.764 ± 0.007	0.80 ± 0.04
DeltoideusScapula_M	0.534 ± 0.006	0.661 ± 0.011	0.529 ± 0.006	0.572 ± 0.018	0.502 ± 0.006	
TRILong	0.885 ± 0.019	0.851 ± 0.01	1.016 ± 0.008	1.003 ± 0.04	1.127 ± 0.015	1.46 ± 0.05
Subscapularis_S	1.023 ± 0.007	1.14 ± 0.004	1.123 ± 0.004	1.162 ± 0.015	1.146 ± 0.007	0.69 ± 0.04
Subscapularis_M	0.924 ± 0.011	1.123 ± 0.006	1.097 ± 0.01	1.157 ± 0.033	1.083 ± 0.019	
Subscapularis_I	1.287 ± 0.007	1.402 ± 0.003	1.393 ± 0.003	1.391 ± 0.013	1.351 ± 0.006	
TrapeziusScapula_M	1.165 ± 0.005	1.444 ± 0.006	1.232 ± 0.004	1.366 ± 0.012	1.135 ± 0.004	0.67 ± 0.08
TrapeziusScapula_S	1.052 ± 0.003	1.259 ± 0.003	1.126 ± 0.002	1.204 ± 0.008	1.099 ± 0.005	
TrapeziusScapula_I	0.966 ± 0.007	1.132 ± 0.007	0.936 ± 0.006	1.059 ± 0.025	0.812 ± 0.01	
TrapeziusClavicle_S	1.016 ± 0.004	1.092 ± 0.003	1.139 ± 0.002	1.126 ± 0.009	1.151 ± 0.007	0.59 ± 0.05

Additionally, the normalized muscle length of Pectoralis Major has been plotted for individual models against coordinates of the glenohumeral joint (Figure 20 – Figure 22).

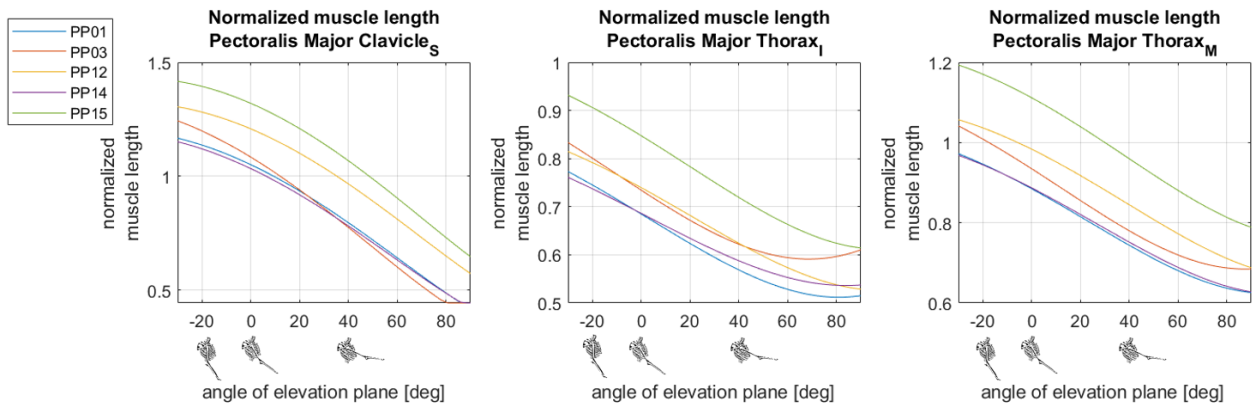


Figure 20: Normalized length of Pectoralis Major at a shoulder elevation angle of 90° against elevation plane coordinate in range of motion of model during pitching

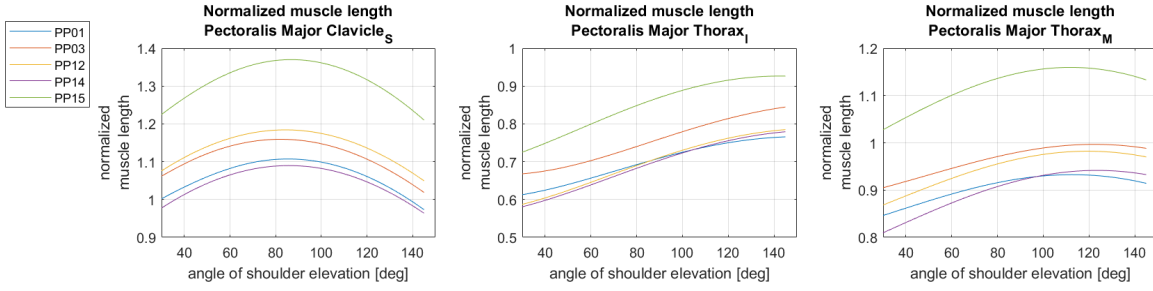


Figure 21: Normalized length of Pectoralis Major against shoulder elevation coordinate in range of motion of model during pitching

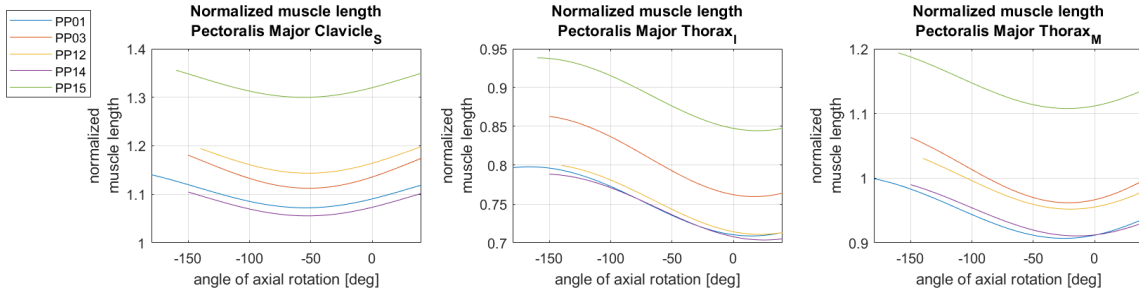


Figure 22: Normalized length of Pectoralis Major at a shoulder elevation angle of 90° against axial rotation coordinate in range of motion of model during pitching

B.3 Fiber velocity calculation

Fibre velocity was calculated using the [Equation 8](#).

$$v_f(t) = \frac{-0.25l(t+2) + 2l(t+1) - 2l(t-1) + 0.25l(t-2)}{3\delta t} \quad (8)$$

B.4 Static optimization

To perform static optimization, the maximal force produced by model muscles needed to be scaled. The scaling factor for all participants was 10, and the maximal isometric forces of the model muscles are presented in [Table 9](#).

Table 9: Maximal isometric force for all participants after scaling with the factor of 10

muscle name	maximal isometric force [N]
TrapeziusScapula_M	4704
TrapeziusScapula_S	10430
TrapeziusScapula_I	4144
TrapeziusClavicle_S	2016
SerratusAnterior_I	4300
SerratusAnterior_M	5080
SerratusAnterior_S	3878
Rhomboideus_S	2002
Rhomboideus_I	4074
LevatorScapulae	2800
Coracobrachialis	6482
DeltoideusClavicle_A	7077
DeltoideusScapula_P	13244
DeltoideusScapula_M	25978
LatissimusDorsi_S	2016
LatissimusDorsi_M	3150
LatissimusDorsi_I	2702
PectoralisMajorClavicle_S	4088
PectoralisMajorThorax_I	5712
PectoralisMajorThorax_M	6832
TeresMajor	8512
Infraspinatus_I	10374
Infraspinatus_S	9674
PectoralisMinor	4298
TeresMinor	6958
Subscapularis_S	5404
Subscapularis_M	6090
Subscapularis_I	8540
Supraspinatus_P	3262
Supraspinatus_A	5432
TRlong	15806
BIC_long	4858
BIC_brevis	6930

B.4.1 Muscle activation

The results of the static optimization for the muscles of interest during the acceleration phase are presented on the ?? - [Figure 27](#).

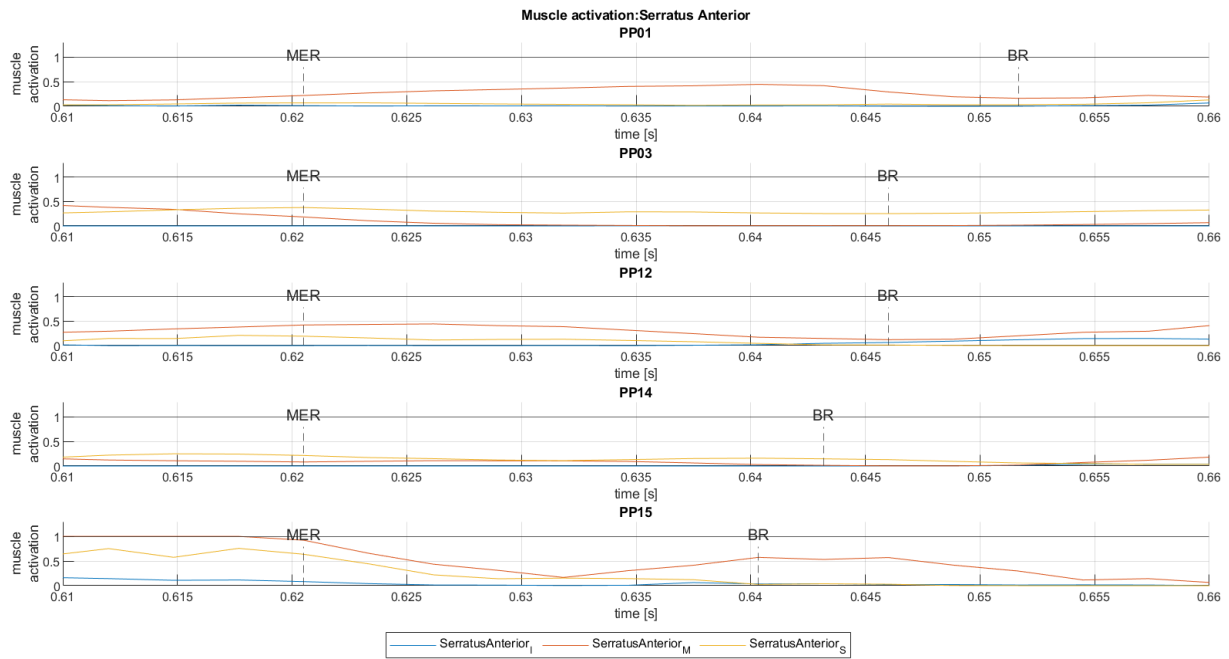


Figure 23: Activation of the Serratus Anterior during the acceleration phase.

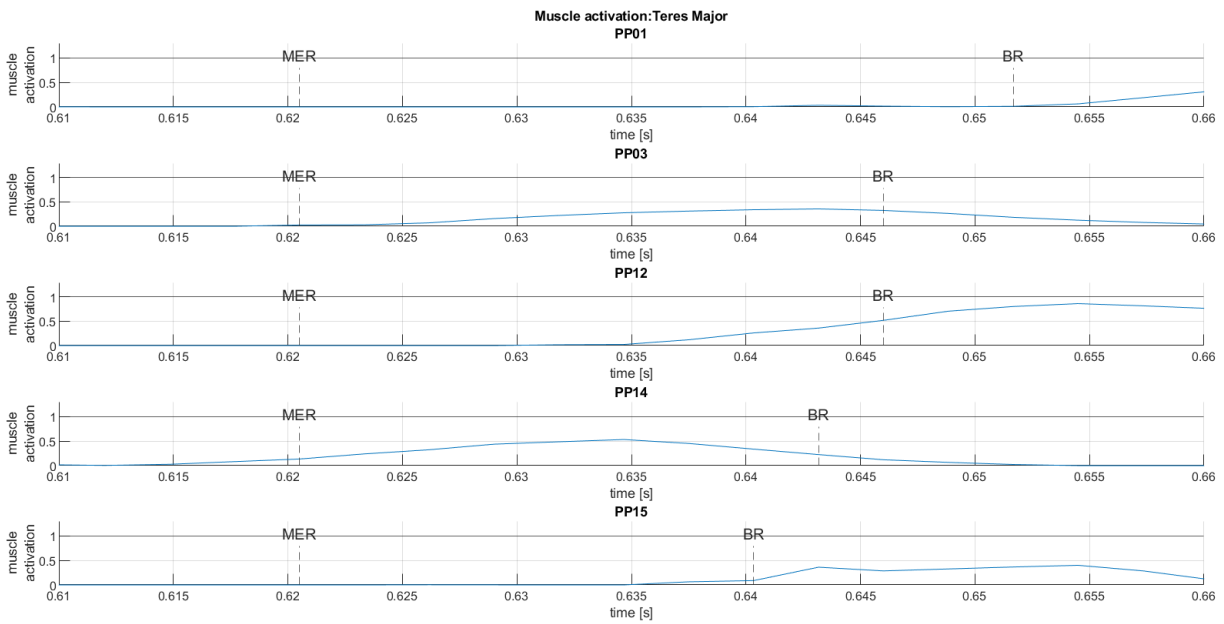


Figure 24: Activation of the Teres Minor during the acceleration phase.

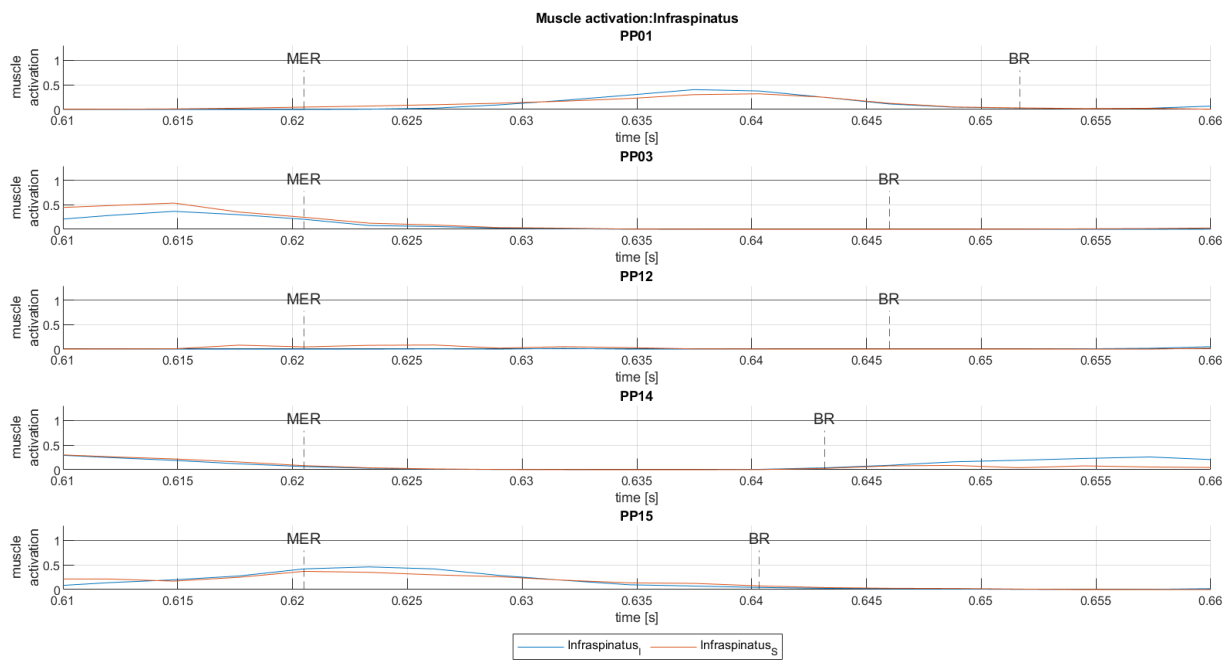


Figure 25: Activation of the Infraspinatus during the acceleration phase.

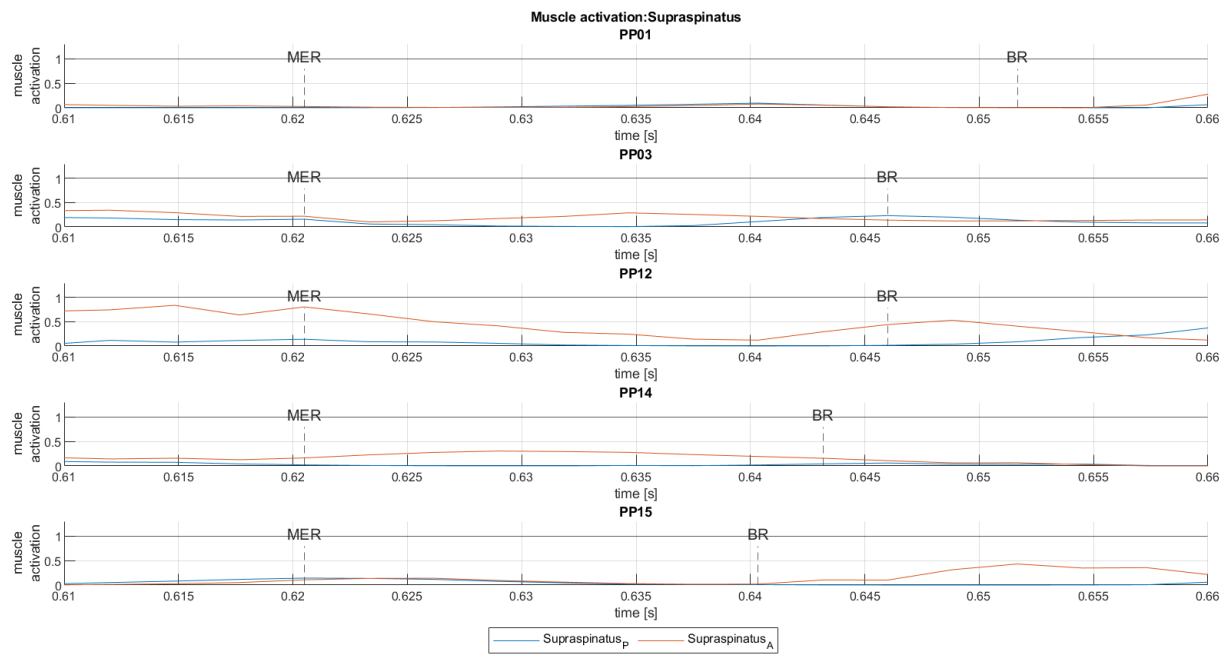


Figure 26: Activation of the Supraspinatus during the acceleration phase.

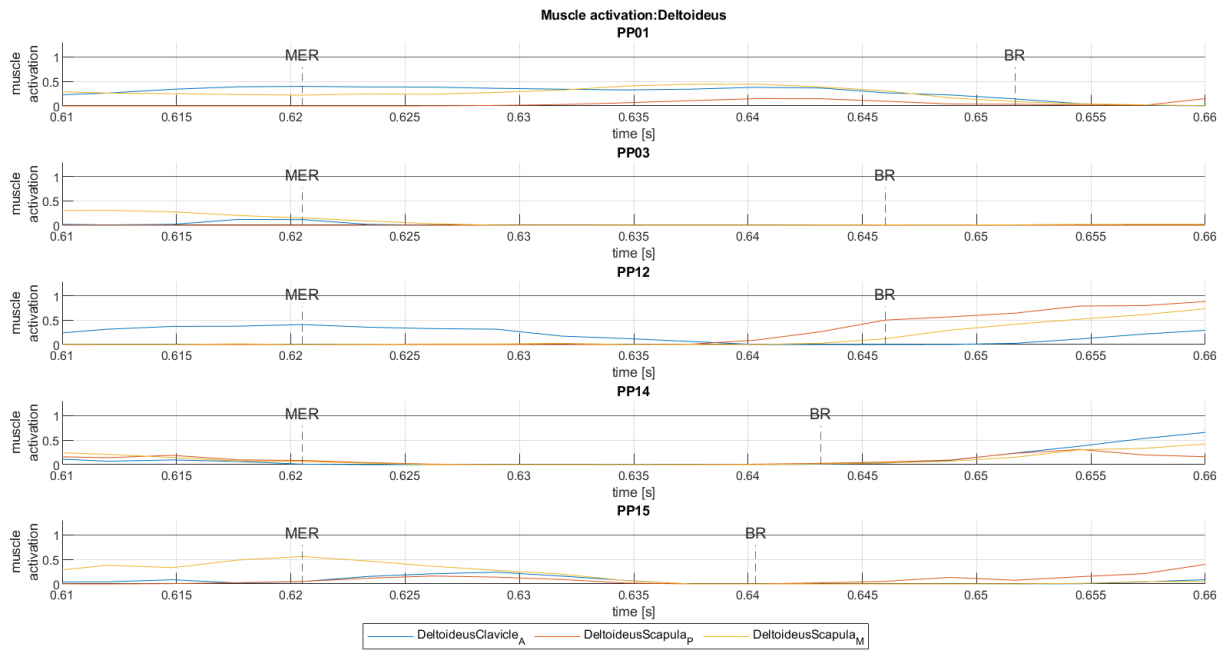


Figure 27: Activation of the Deltoides muscle during the acceleration phase.

B.4.2 Torque

The method of torque calculation is presented in [subsubsection 2.3.5](#). The focus of the presented research is the glenohumeral joint during the acceleration phase. To check if the calculated torque produced by the pectoralis major muscle is correct, there is a necessity to compare its contribution with the total torque in the joint. The torque for all muscles acting in the glenohumeral joint has been calculated and presented in [Figure 28 - Figure 32](#).

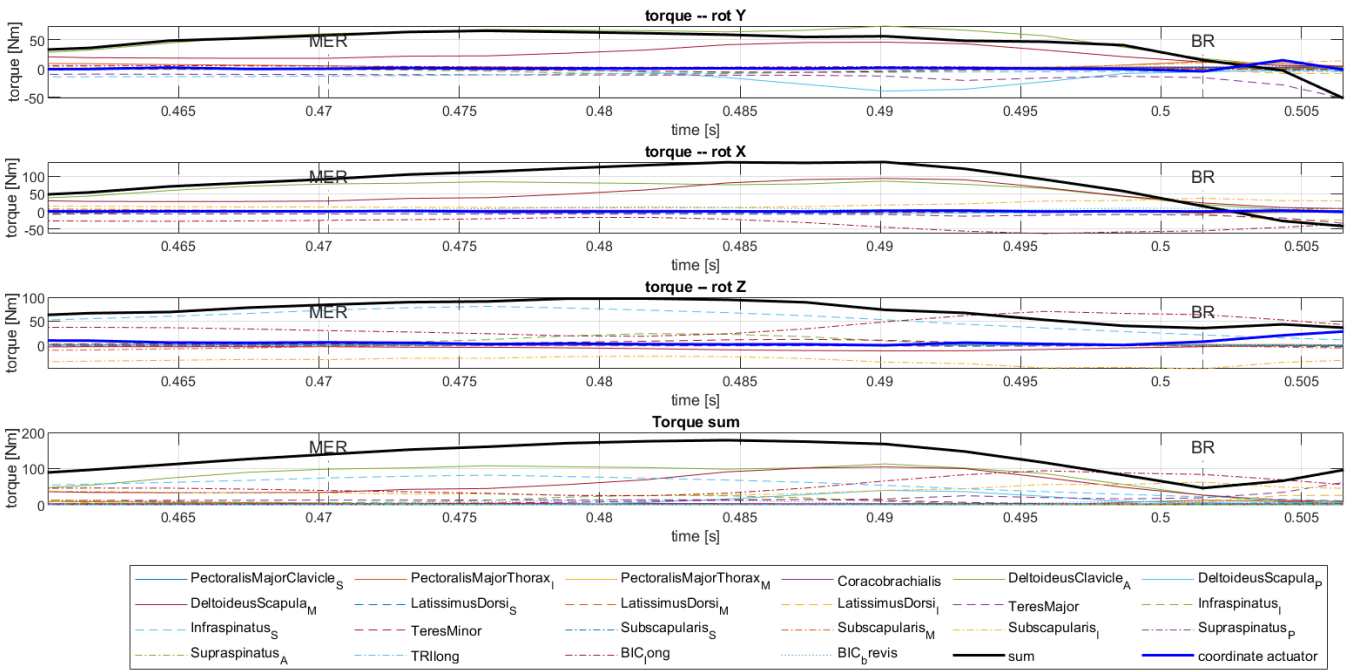


Figure 28: Participant 01. Contribution of muscles to total torque in the glenohumeral joint during the acceleration phase. From top: torque acting around Y axis; torque acting around X axis; torque around Z axis; total torque in joint

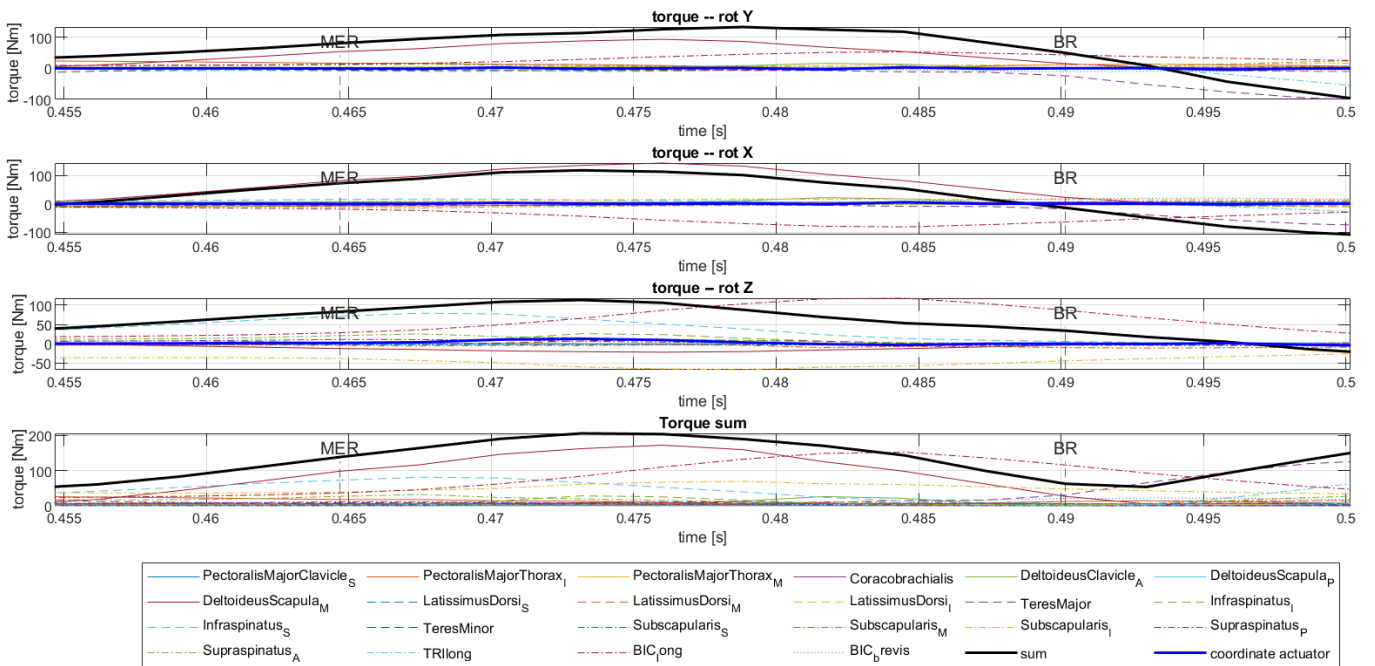


Figure 29: Participant 03. Contribution of muscles to total torque in the glenohumeral joint during the acceleration phase. From top: torque acting around Y axis; torque acting around X axis; torque around Z axis; total torque in joint

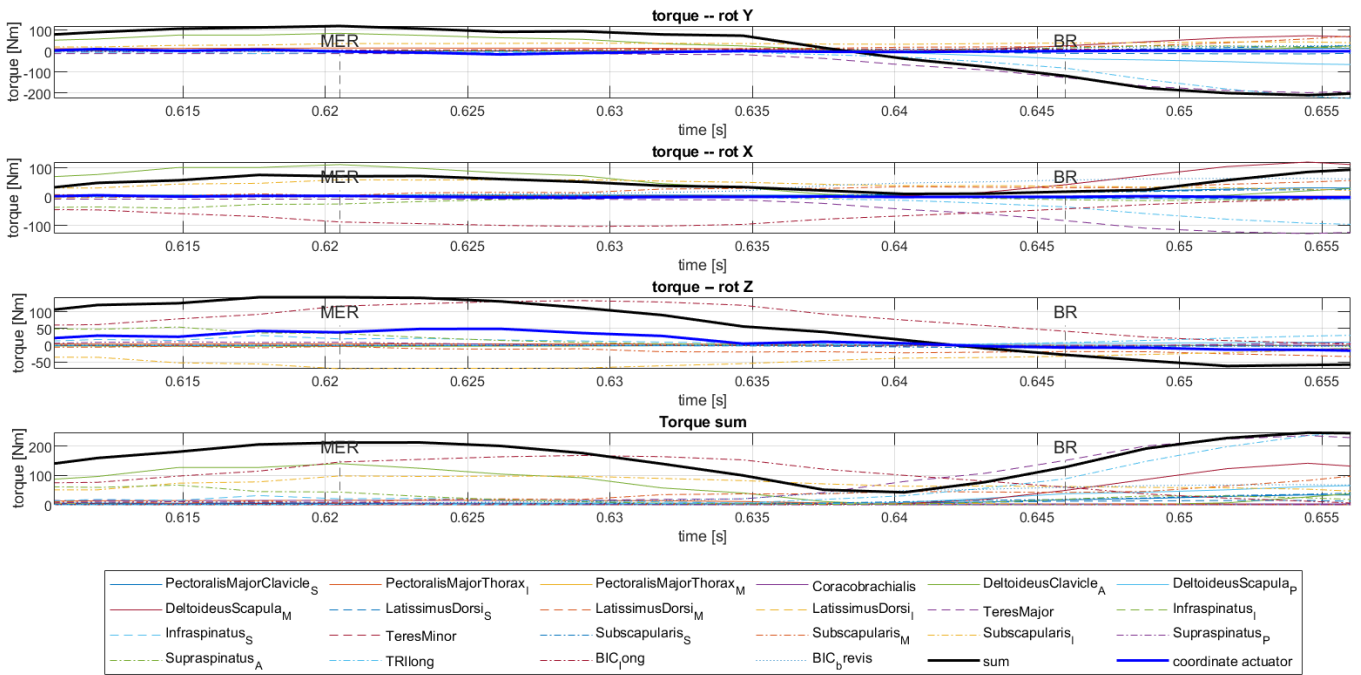


Figure 30: Participant 12. Contribution of muscles to total torque in the glenohumeral joint during the acceleration phase. From top: torque acting around Y axis; torque acting around X axis; torque around Z axis; total torque in joint

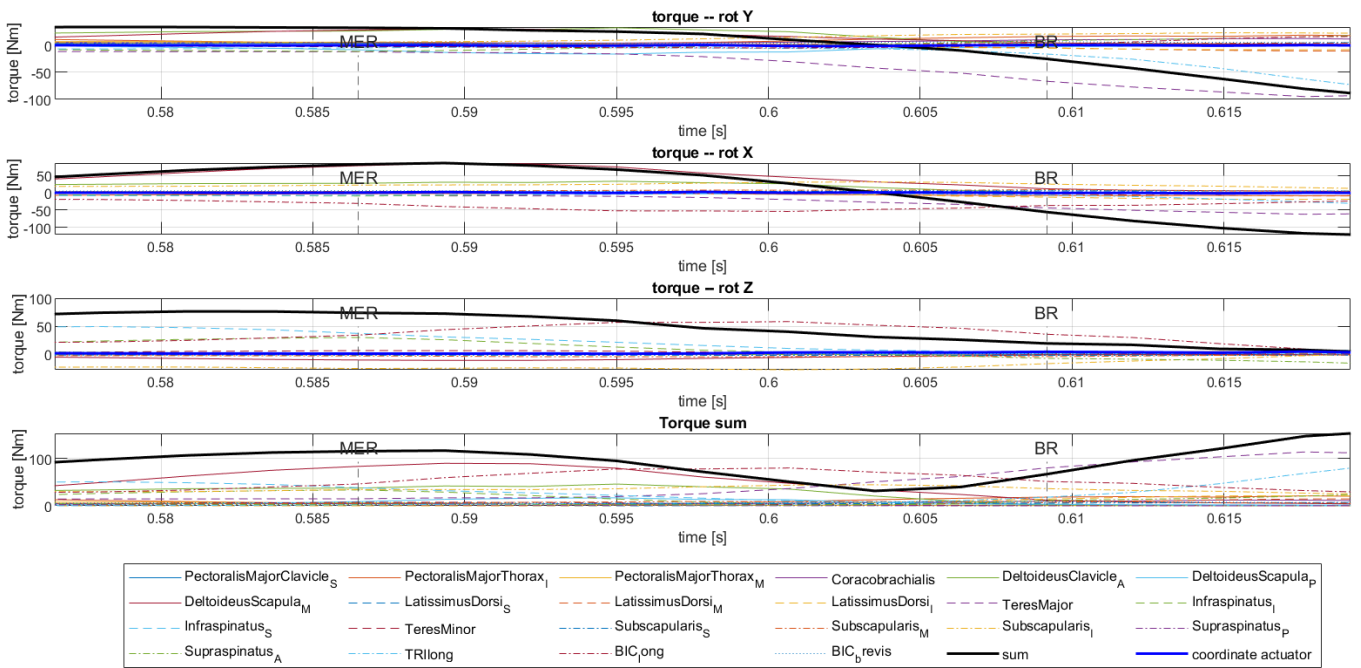


Figure 31: Participant 14. Contribution of muscles to total torque in the glenohumeral joint during the acceleration phase. From top: torque acting around Y axis; torque acting around X axis; torque around Z axis; total torque in joint

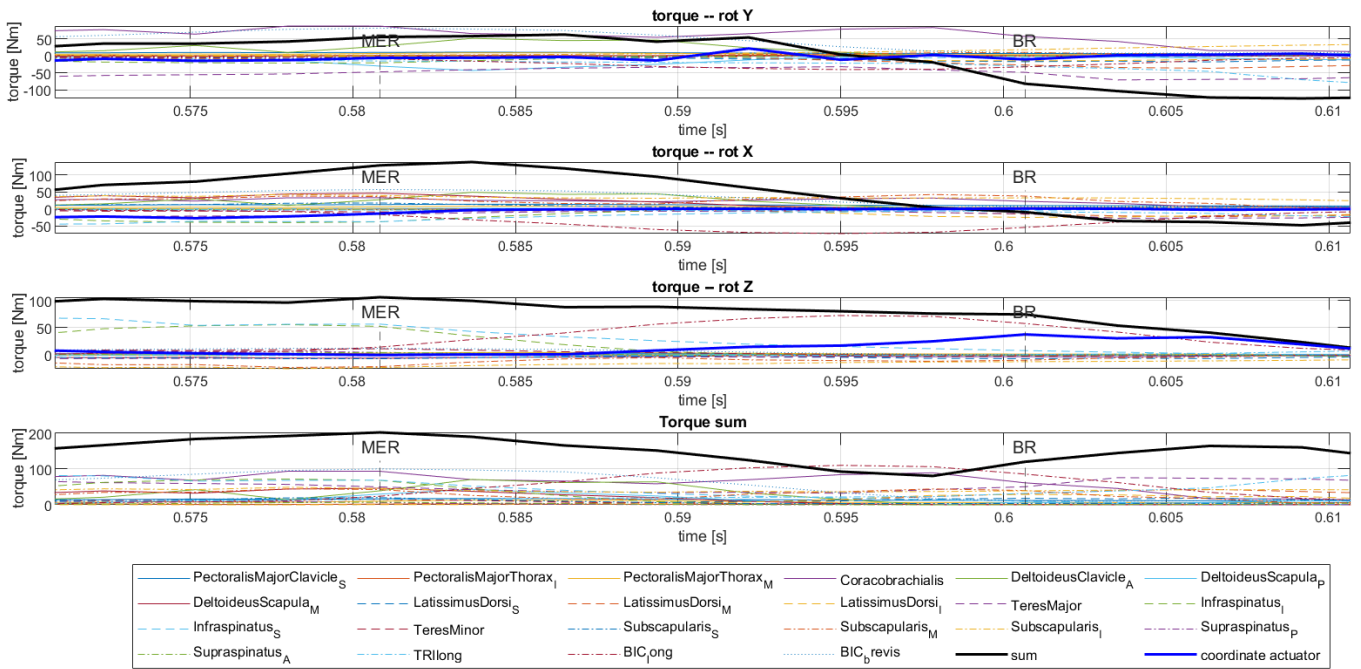


Figure 32: Participant 15. Contribution of muscles to total torque in the glenohumeral joint during the acceleration phase. From top: torque acting around Y axis; torque acting around X axis; torque around Z axis; total torque in joint

To evaluate torque is also needed to analyse the moment arm of the muscles of interest (Pectoralis Major). The moment arm has been evaluated for all participants at *shoulder elevation* angle of 90° in the glenohumeral joint (Figure 33 - Figure 35).

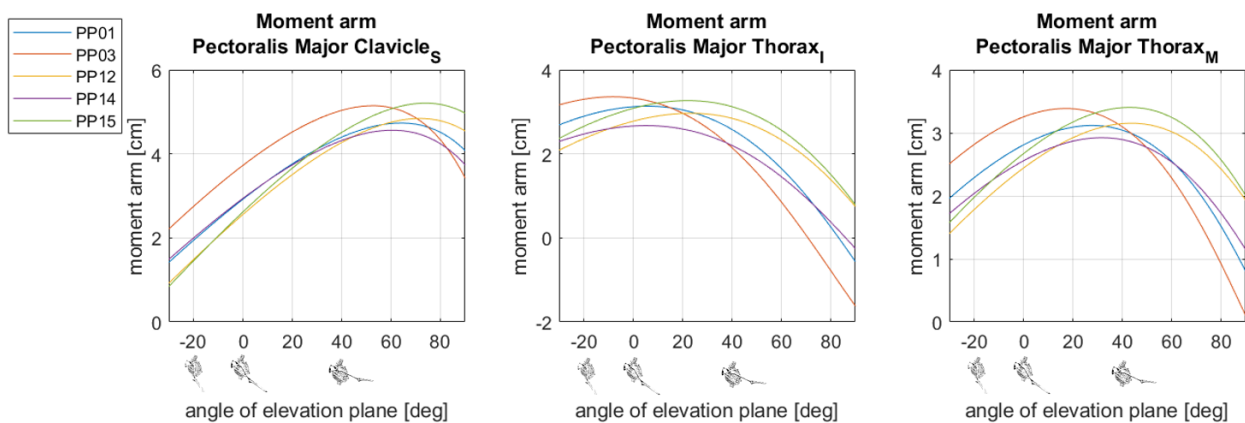


Figure 33: Moment arm of pectoralis major for elevation plane, measured at 90° of shoulder elevation angle

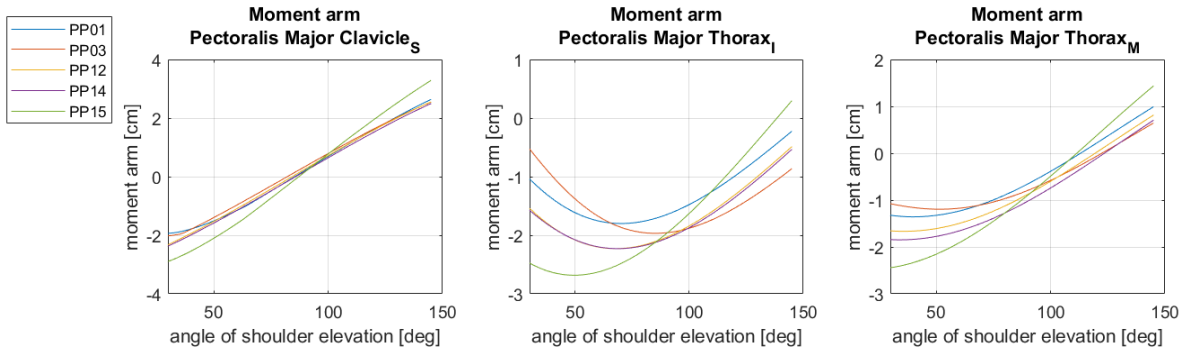


Figure 34: Moment arm of Pectoralis Major for shoulder elevation torque

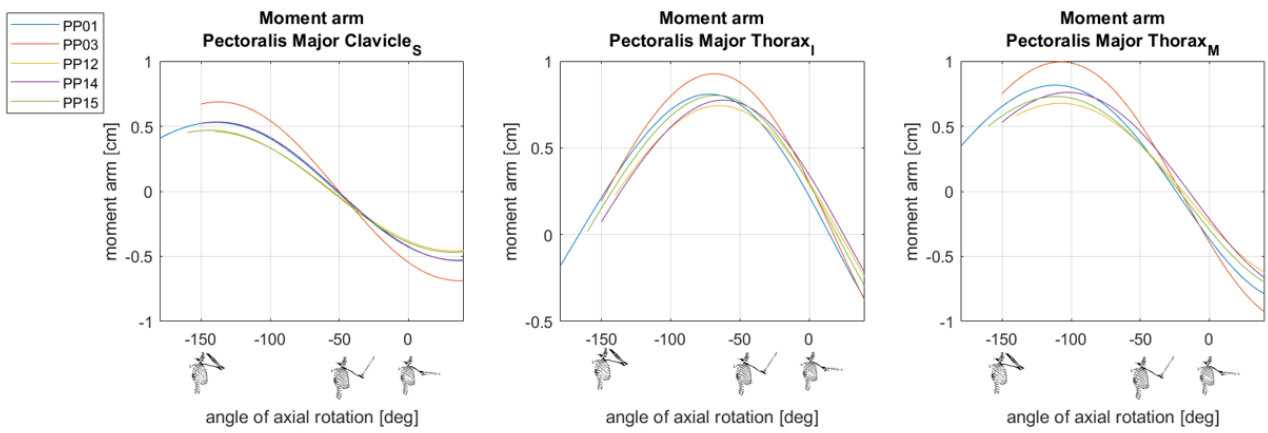


Figure 35: Moment arm of Pectoralis Major for axial rotation torque, measured at 90° of shoulder elevation angle and elevation plane angle of 0°.

B.4.3 Coordinate actuators

To ensure that model is able to perform the desired motion and muscle activation can be computed with the use of the static optimization, the coordinate actuators were added to the model. A list of the actuators with properties is presented in the [Table 10](#) and the resulted torque from the actuators for each participant is presented in [Figure 36](#) - [Figure 40](#).

Table 10: List of the coordinate actuators added to the model. Explanation of the coordinate names can be found in Table 1

Coordinate name	Optimal force	Min value of control signal	Max value of control signal
ground_thorax_rot_x	1000	$-\infty$	∞
ground_thorax_rot_y	1000	$-\infty$	∞
ground_thorax_rot_z	1000	$-\infty$	∞
ground_thorax_tx	1000	$-\infty$	∞
ground_thorax_ty	1000	$-\infty$	∞
ground_thorax_tz	1000	$-\infty$	∞
elbow_flexion	100	$-\infty$	∞
pro_sup	100	$-\infty$	∞
clav_prot	100	$-\infty$	∞
clav_elev	100	$-\infty$	∞
scapula_abduction	100	$-\infty$	∞
scapula_elevation	100	$-\infty$	∞
scapula_upward_rot	100	$-\infty$	∞
scapula_winging	100	$-\infty$	∞
plane_elv	100	$-\infty$	∞
shoulder_elv	100	$-\infty$	∞
axial_rot	100	$-\infty$	∞

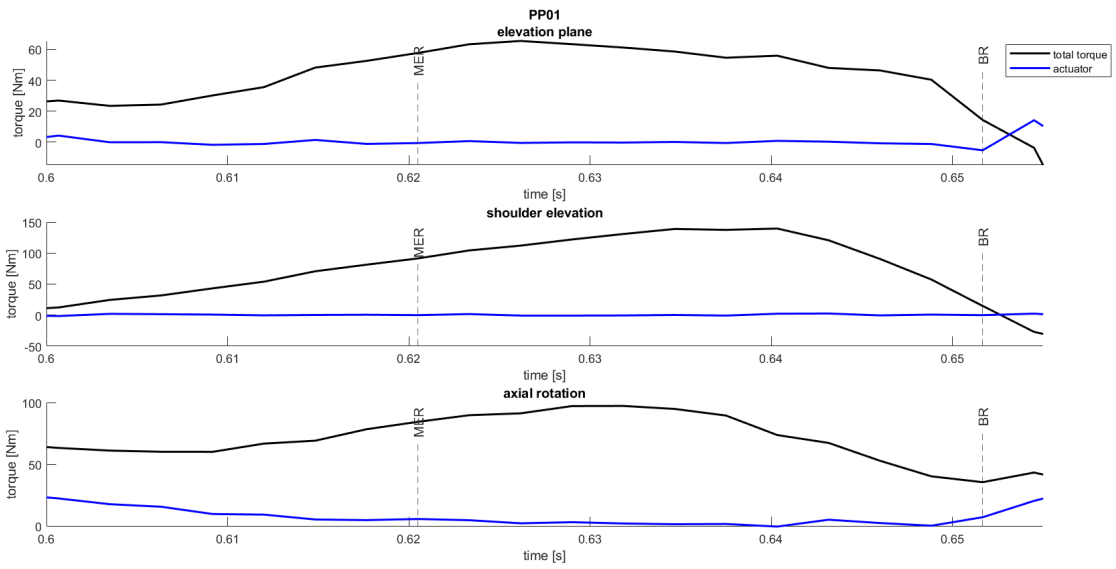


Figure 36: PP01: torque produced by the coordinate actuators compared with the total torque.

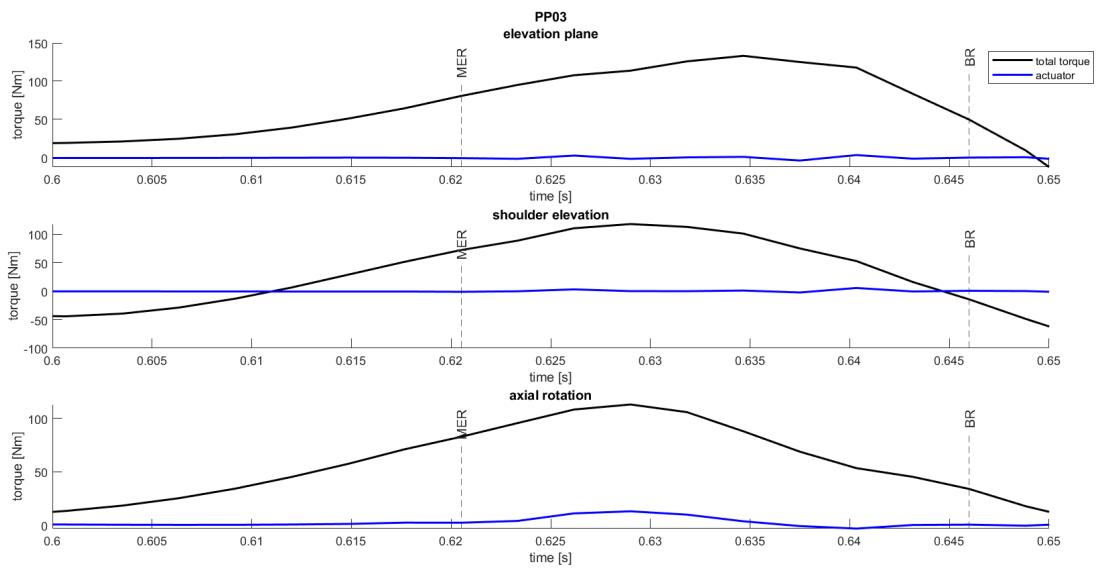


Figure 37: PP03: torque produced by the coordinate actuators compared with the total torque.

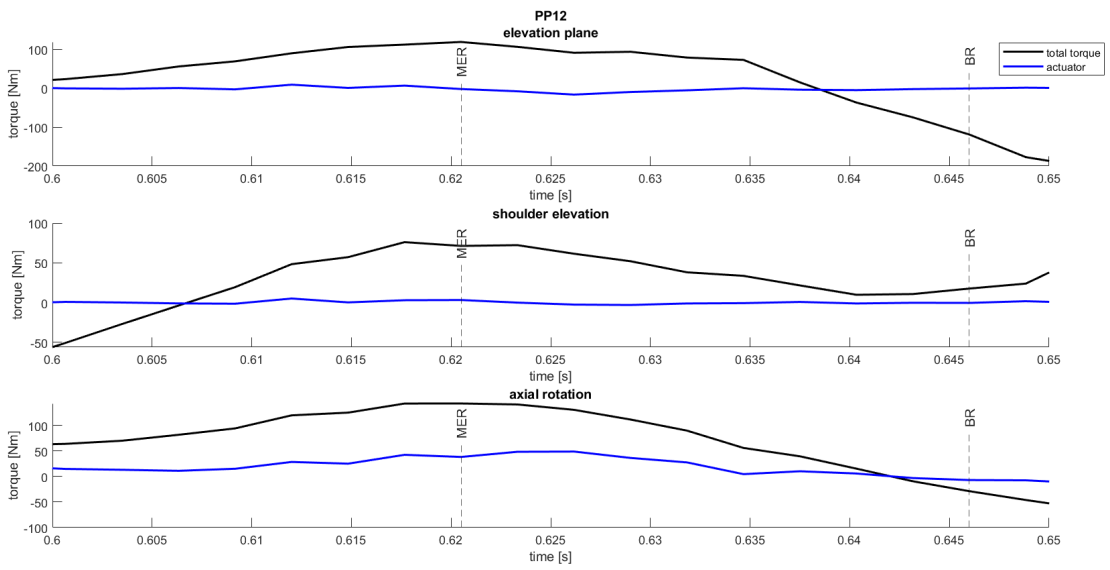


Figure 38: PP12: torque produced by the coordinate actuators compared with the total torque.

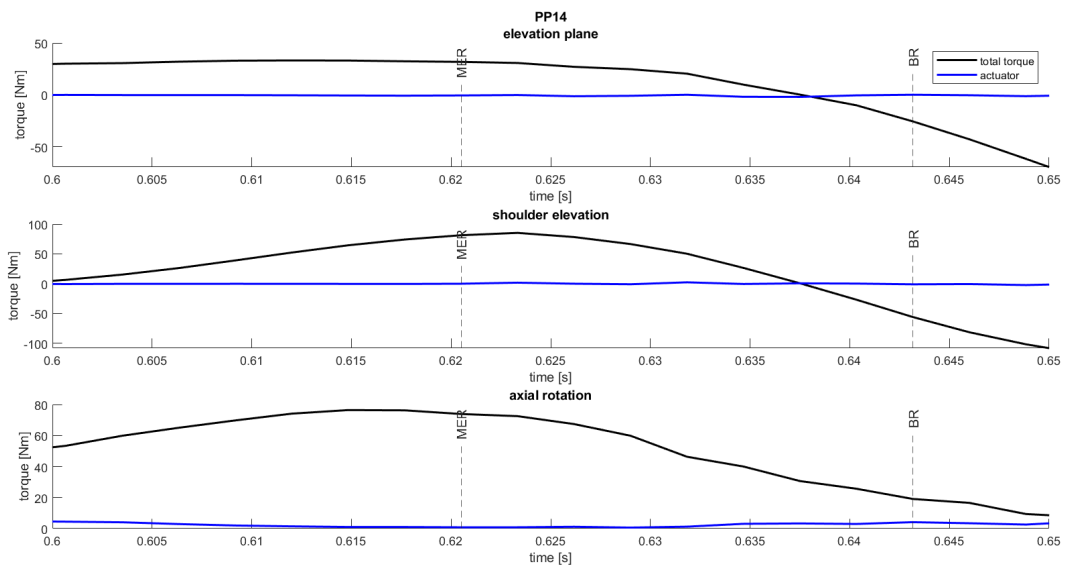


Figure 39: PP14: torque produced by the coordinate actuators compared with the total torque.

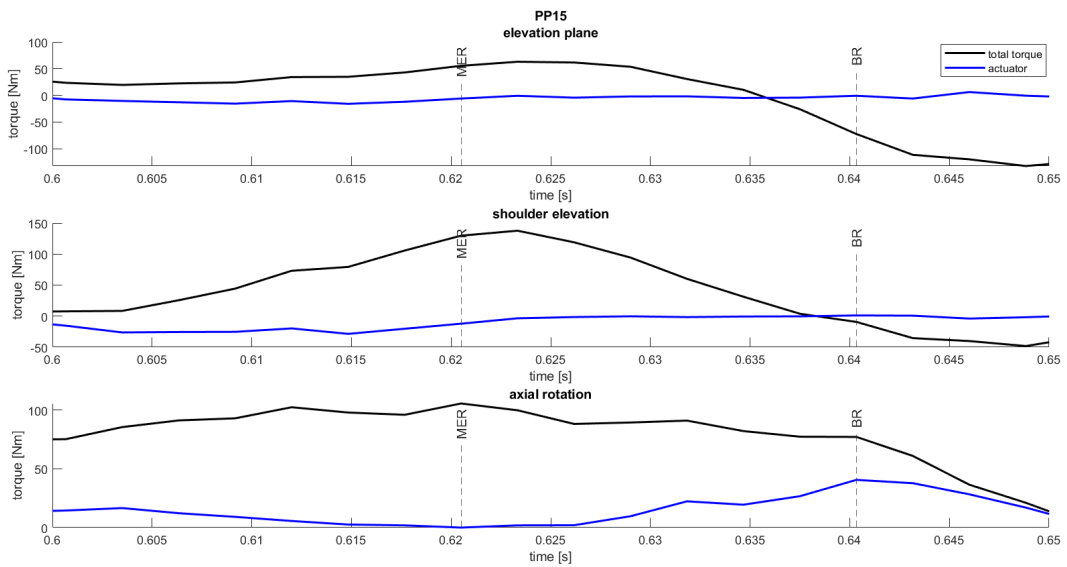


Figure 40: PP15: torque produced by the coordinate actuators compared with the total torque.

B.4.4 Changes in pectoralis major length

The torque in the glenohumeral joint during the acceleration phase for participant 3 with 20% and 50% shorter pectoralis major muscles is presented in Figure 41 and Figure 42 respectively.

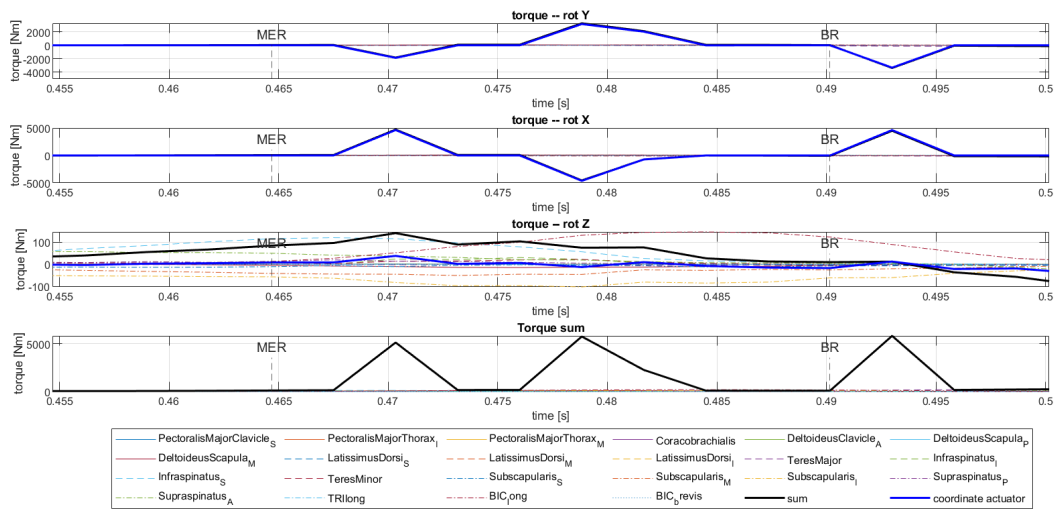


Figure 41: PP03 with shorter thorax part of pectoralis major by 20%. Contribution of the muscles to the torque in the glenohumeral joint.

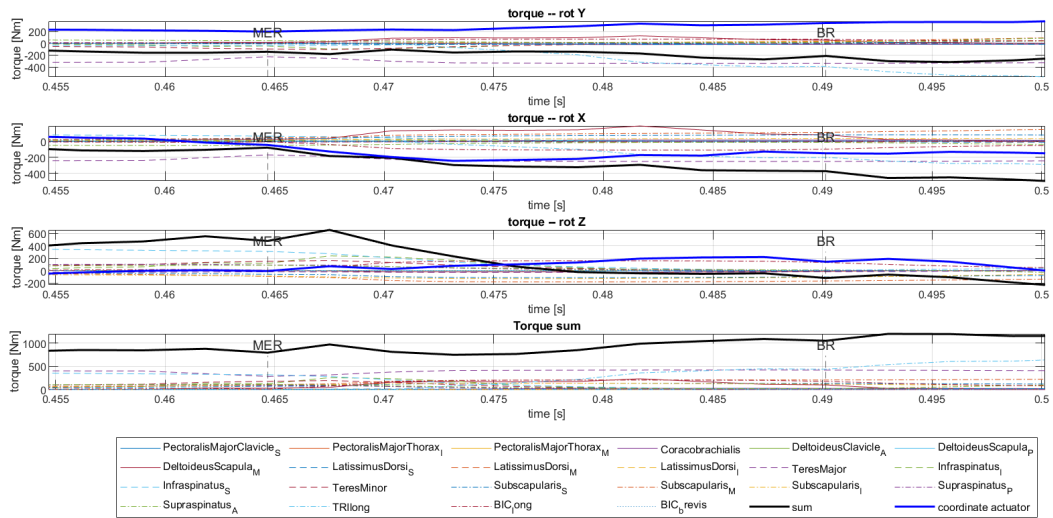
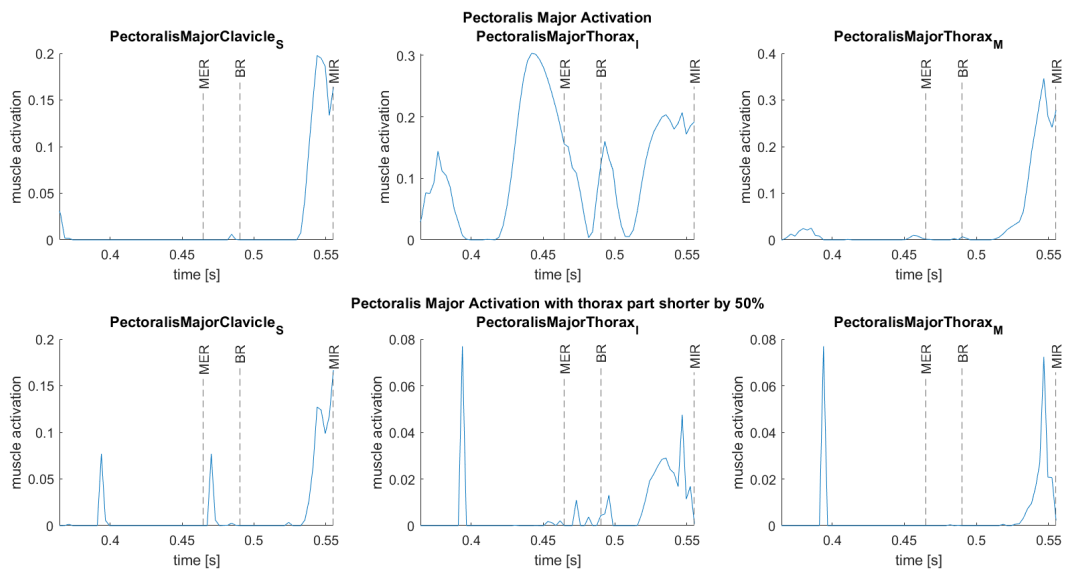
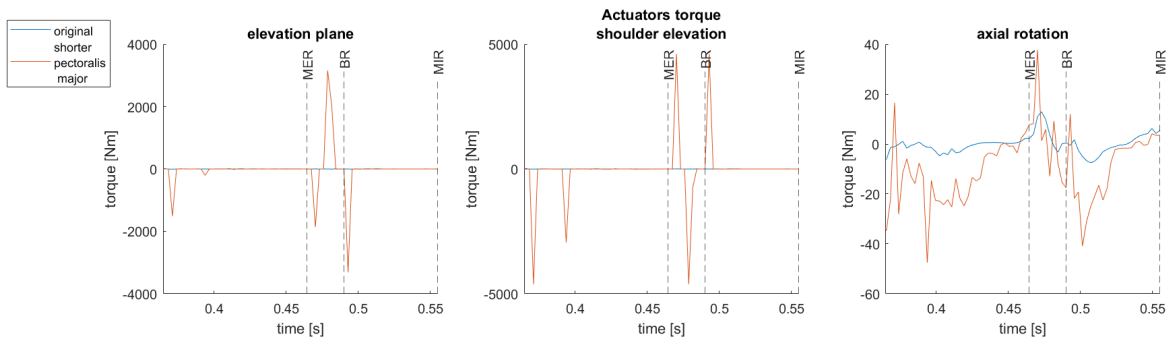


Figure 42: PP03 with shorter thorax part of pectoralis major by 50%. Contribution of the muscles to the torque in the glenohumeral joint.

The results of the static optimization for modified models are compared with the results of SO for the original model and presented in [Figure 43](#) and [Figure 44](#).

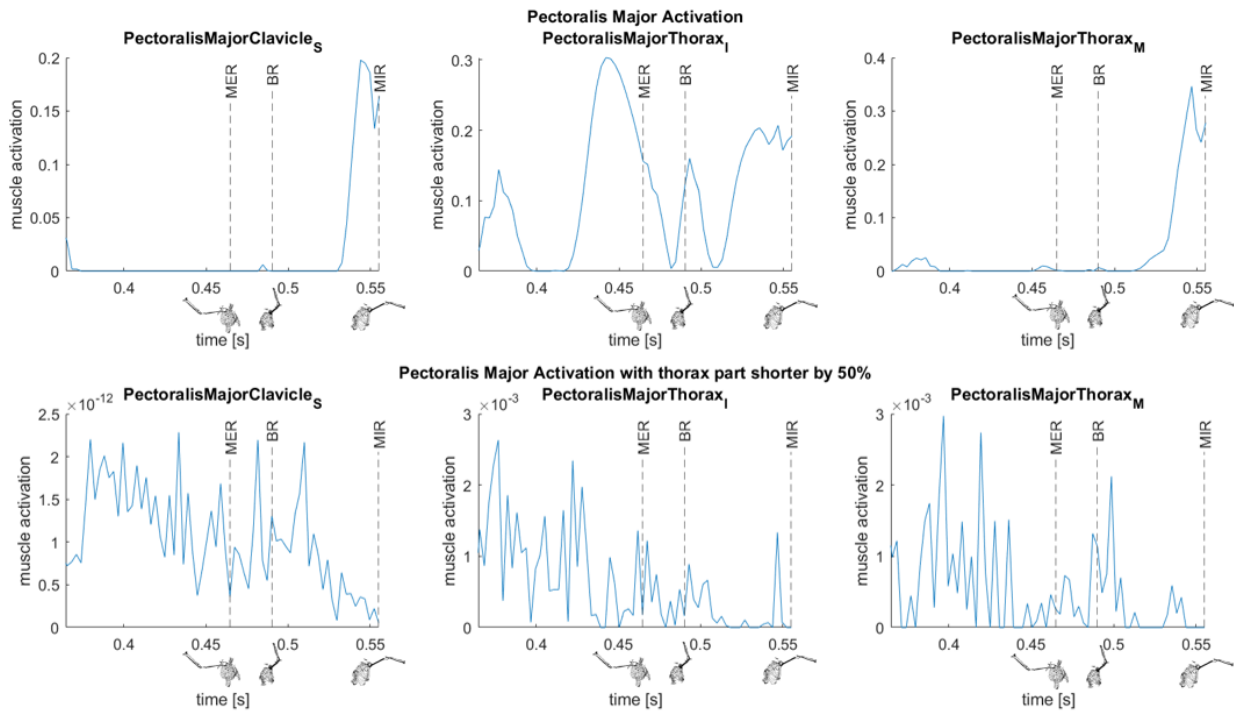


(a) Activation of pectoralis major during pitching.

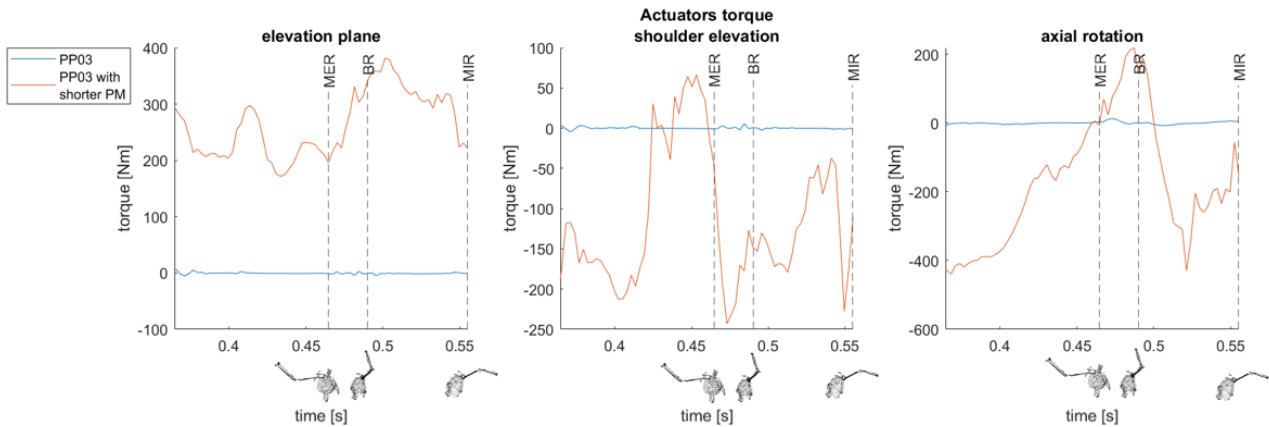


(b) Torque produced by the coordinate actuators

Figure 43: Comparison between results of static optimization for participant 3 and participant 3 with shortened pectoralis major thorax part by 20%.



(a) Activation of pectoralis major during pitching.



(b) Torque produced by the coordinate actuators

Figure 44: Comparison between results of static optimization for participant 3 and participant 3 with shortened pectoralis major thorax part by 50%.

C Acceleration alignment

The alignment using acceleration data was challenging because only one channel from the accelerometer was saved. It was decided to save the data regarding acceleration in the forward direction. The forward direction for measured data is along the X-axis. EMG measurements were aligned with the OpenSim kinematic results using the X component of the acceleration of the IJ marker. Before alignment, both data sets were scaled, by dividing the data sets by their standard deviation. The results of the alignment for all participants are presented below. Additionally, the absolute value of the raw EMG signal is presented, aligned with the static optimization results and fibre velocity of chosen muscles.

C.1 PP01

The alignment of the acceleration data for participant 1 is presented in [Figure 48](#). The comparison of the EMG signal with muscle activity computed with static optimization algorithm and with muscle's fiber velocity is presented in [Figure 46](#), for Pectoralis Major, and in [Figure 47](#), for the Deltoideus and Latissimus Dorsi.

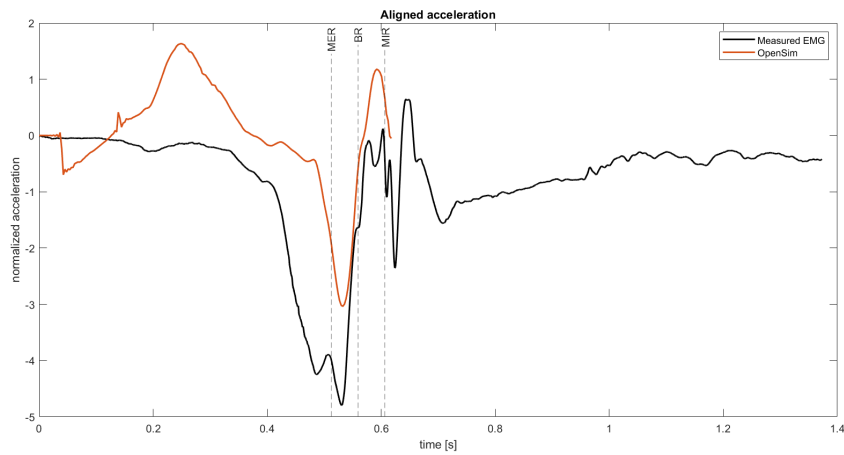


Figure 45: Alignment of acceleration data for PP01

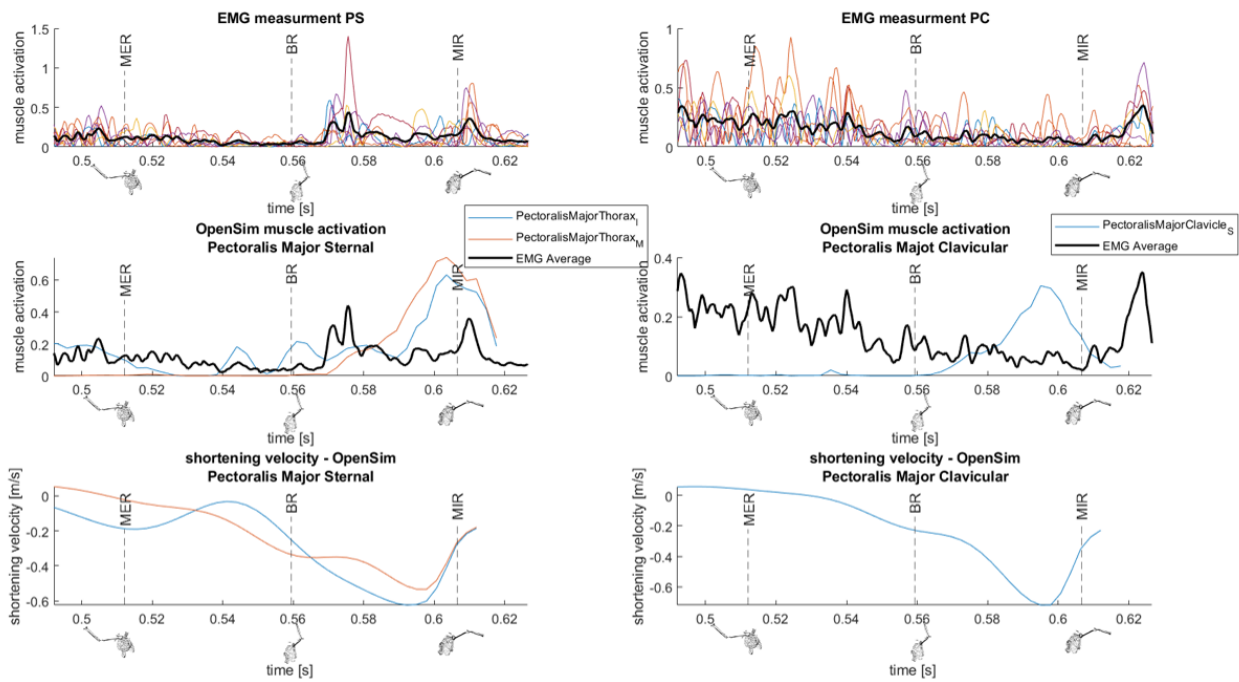


Figure 46: PP01: Comparison between muscle activity measured for Pectoralis Major and data obtained from static optimization, and fiber velocity computed based on the kinematics of the OpenSim model.

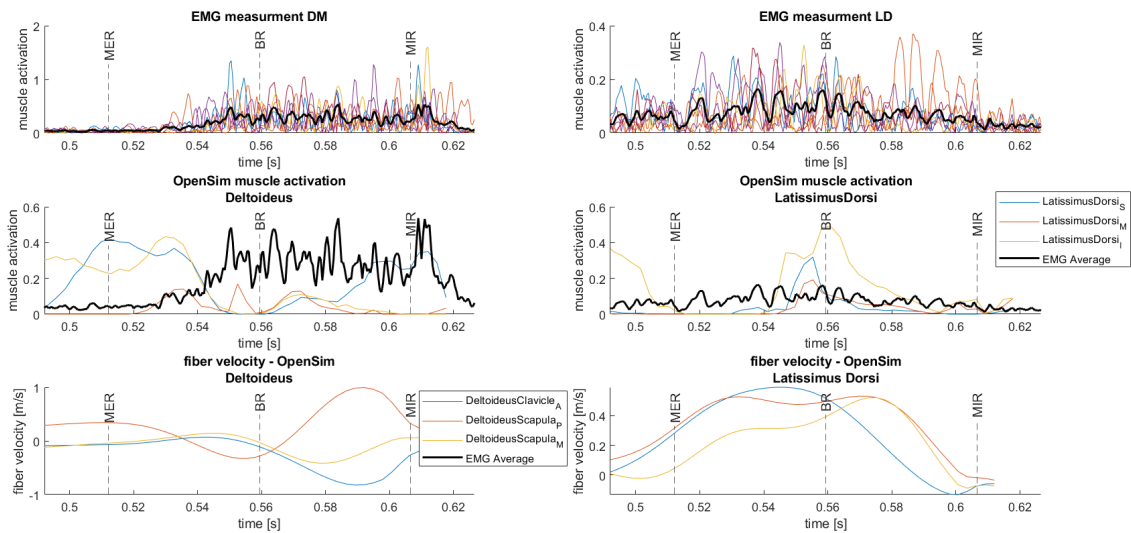


Figure 47: PP01: Comparison between muscle activity measured, for Deltoid muscle and Latissimus Dorsi, and data obtained from static optimization, and fiber velocity computed based on the kinematics of the OpenSim model.

C.2 PP03

The alignment of the acceleration data for participant 3 is presented in ???. The comparison of the EMG signal with muscle activity computed with static optimization algorithm and with muscle's fiber velocity is presented in Figure 49, for Pectoralis Major, and in Figure 50, for the Deltoideus and Latissimus Dorsi.

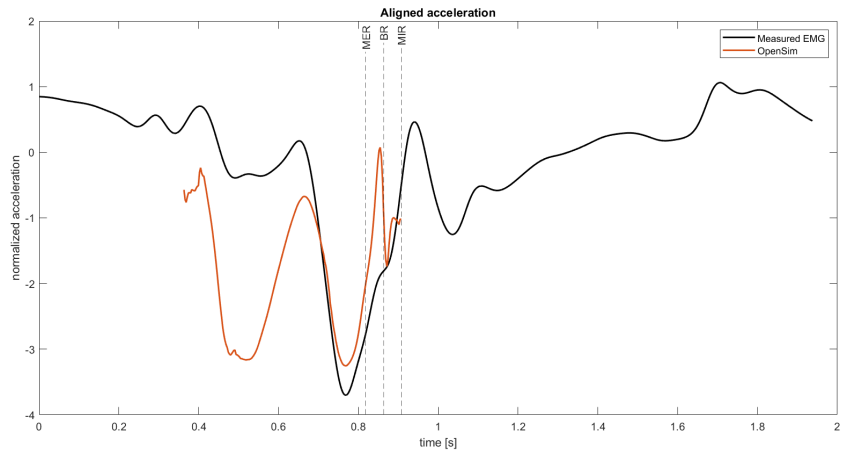


Figure 48: Alignment of acceleration data for PP03

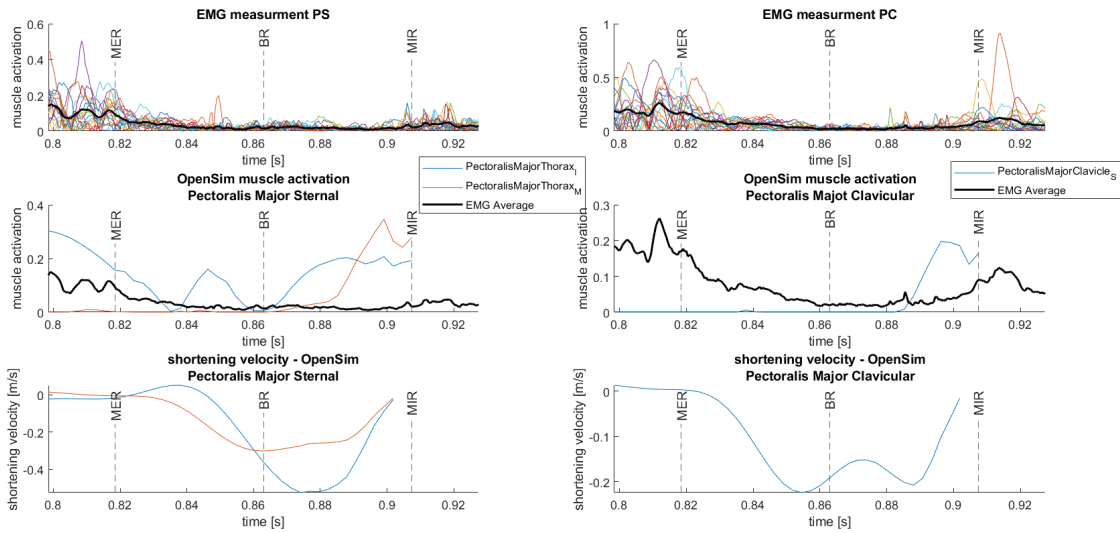


Figure 49: PP03: Comparison between muscle activity measured for Pectoralis Major and data obtained from static optimization, and fiber velocity computed based on the kinematics of the OpenSim model.

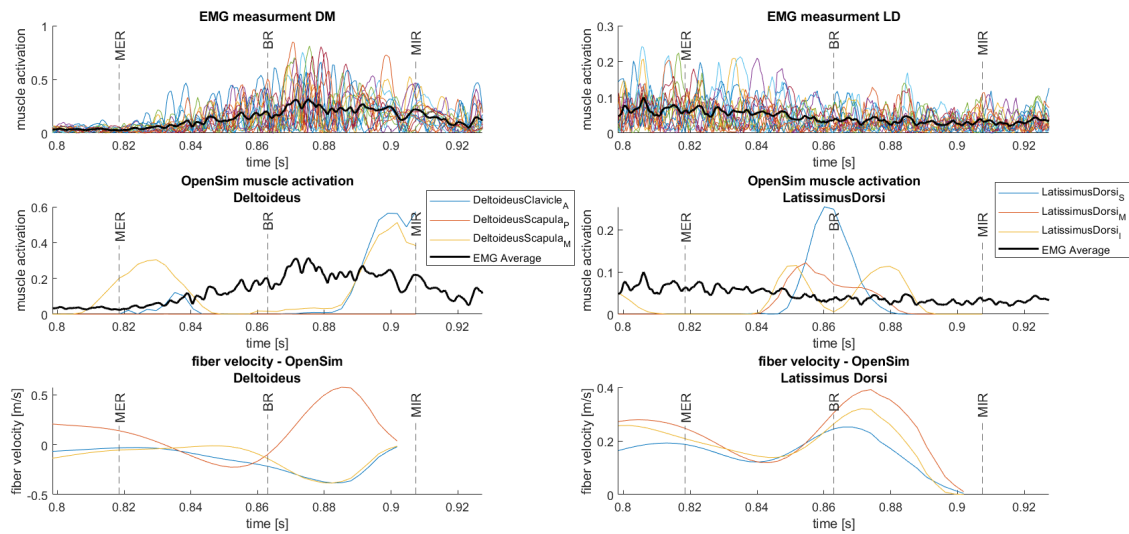


Figure 50: PP03: Comparison between muscle activity measured, for Deltoid muscle and Latissimus Dorsi, and data obtained from static optimization, and fiber velocity computed based on the kinematics of the OpenSim model.

C.3 PP12

The alignment of the acceleration data for participant 1 is presented in Figure 51. The comparison of the EMG signal with muscle activity computed with static optimization algorithm and with muscle's fiber velocity is presented in Figure 52, for Pectoralis Major, and in Figure 53, for the Deltoides and Latissimus Dorsi.

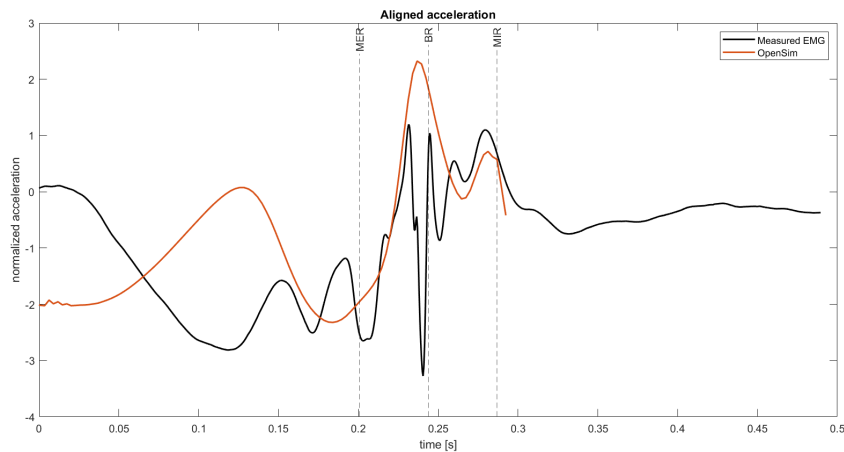


Figure 51: Alignment of acceleration data for PP12

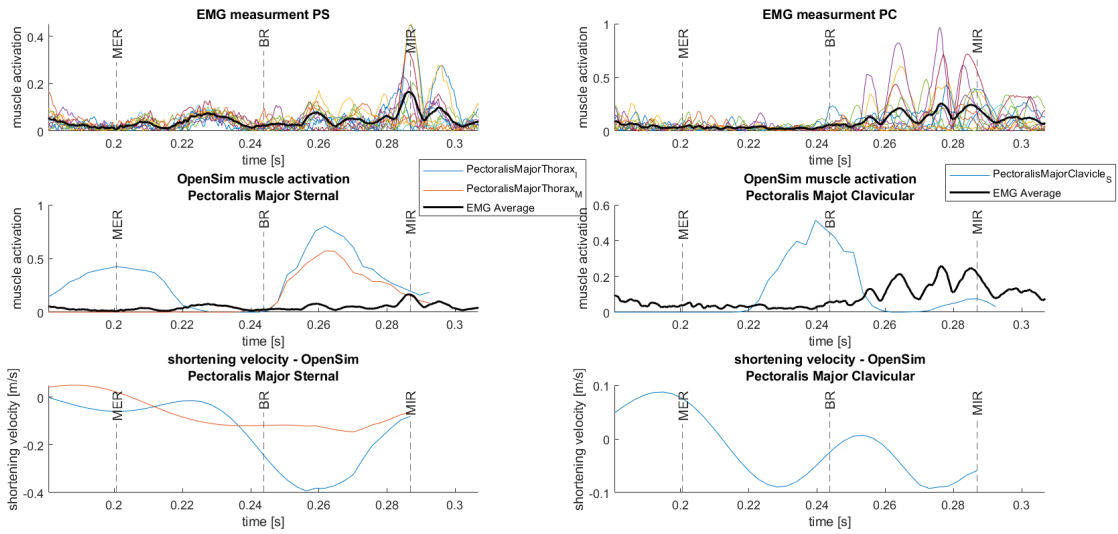


Figure 52: PP12: Comparison between muscle activity measured for Pectoralis Major and data obtained from static optimization, and fiber velocity computed based on the kinematics of the OpenSim model.

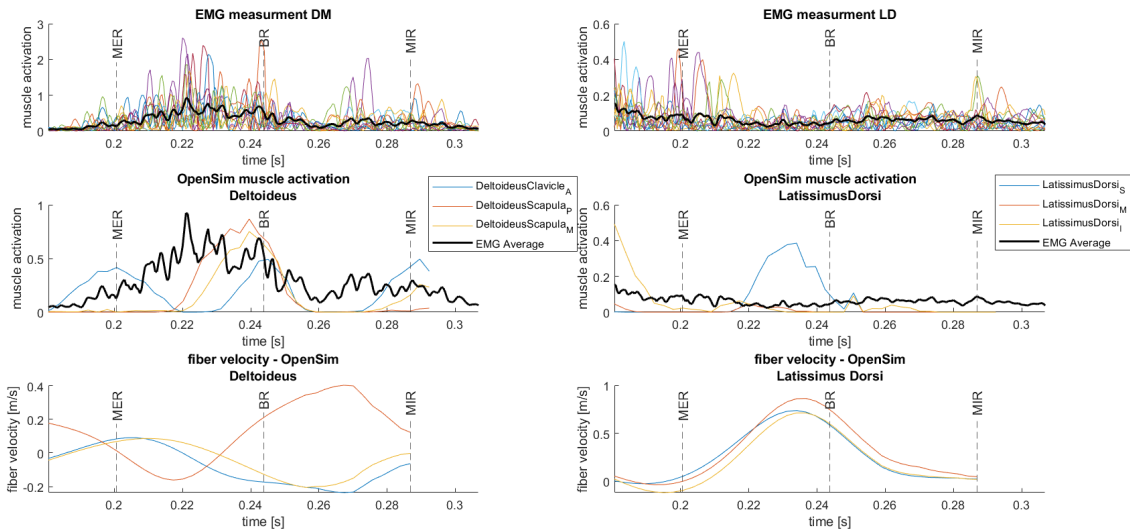


Figure 53: PP12: Comparison between muscle activity measured, for Deltoid muscle and Latissimus Dorsi, and data obtained from static optimization, and fiber velocity computed based on the kinematics of the OpenSim model.

C.4 PP14

The alignment of the acceleration data for participant 1 is presented in [Figure 54](#). The comparison of the EMG signal with muscle activity computed with static optimization algorithm and with muscle's fiber velocity is presented in [Figure 55](#), for Pectoralis Major, and in [Figure 56](#), for the Deltoides and Latissimus Dorsi.

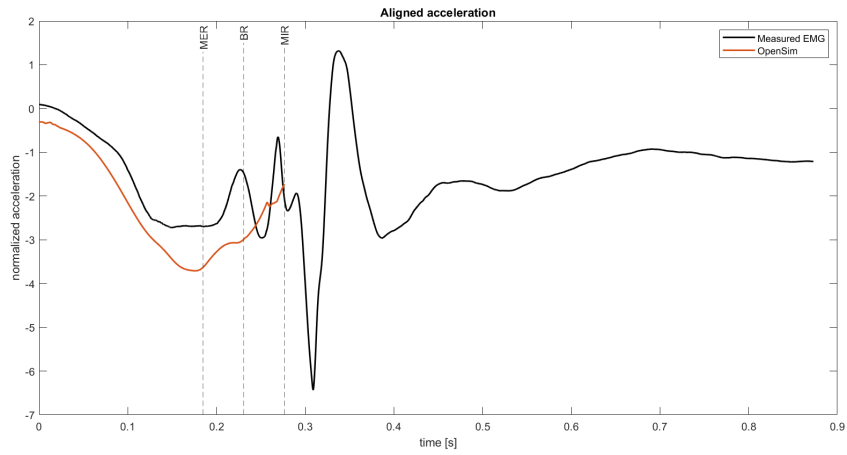


Figure 54: Alignment of acceleration data for PP14

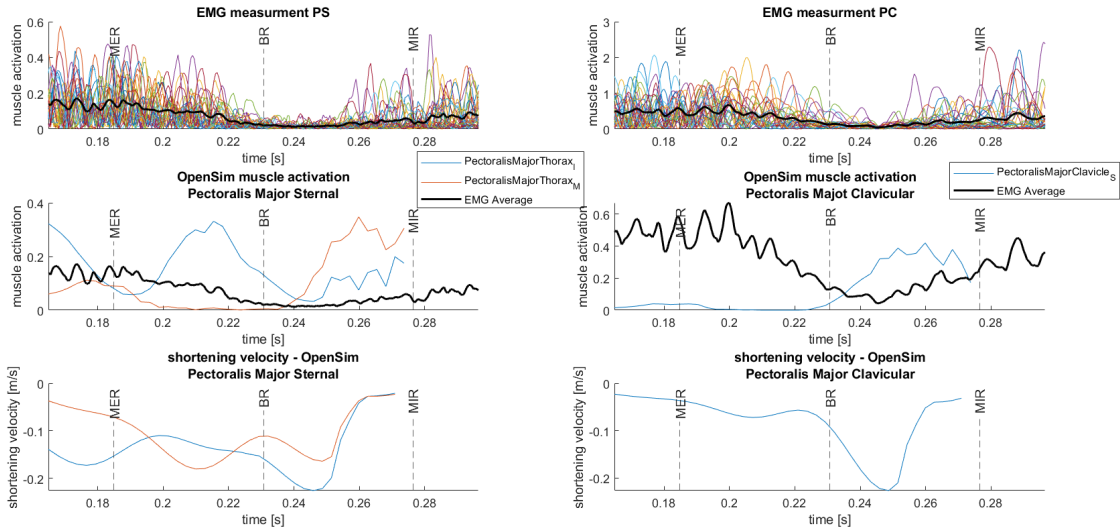


Figure 55: PP14: Comparison between muscle activity measured for Pectoralis Major and data obtained from static optimization, and fiber velocity computed based on the kinematics of the OpenSim model.

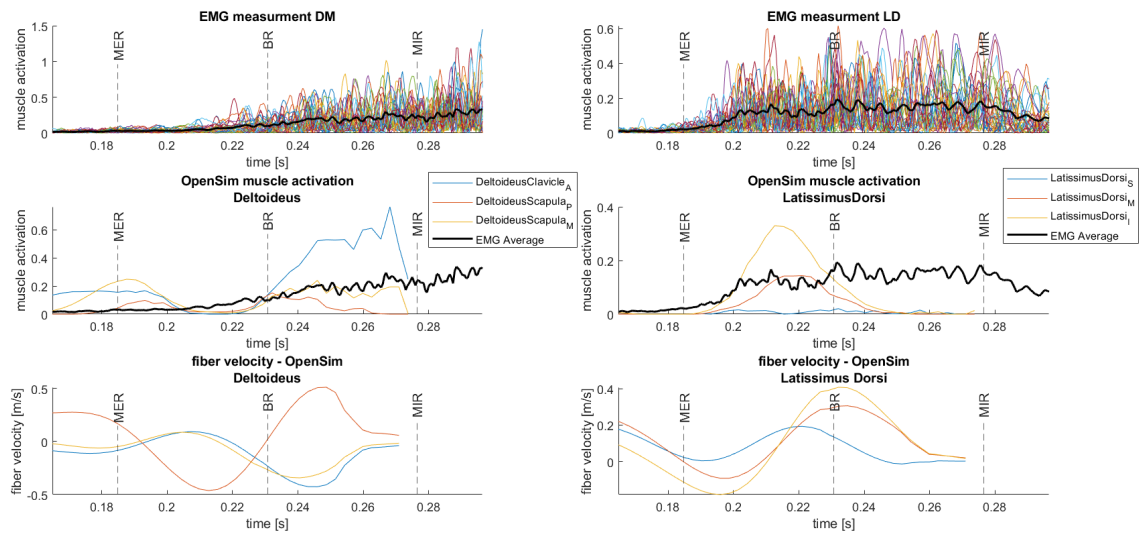


Figure 56: PP14: Comparison between muscle activity measured, for Deltoid muscle and Latissimus Dorsi, and data obtained from static optimization, and fiber velocity computed based on the kinematics of the OpenSim model.

C.5 PP15

The alignment of the acceleration data for participant 1 is presented in Figure 57. The comparison of the EMG signal with muscle activity computed with static optimization algorithm and with muscle's fiber velocity is presented in Figure 58, for Pectoralis Major, and in Figure 59, for the Deltoides and Latissimus Dorsi.

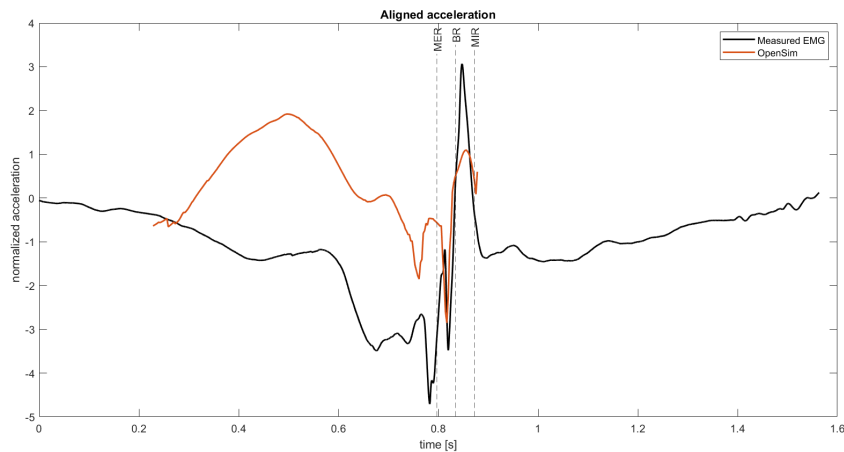


Figure 57: Alignment of acceleration data for PP15

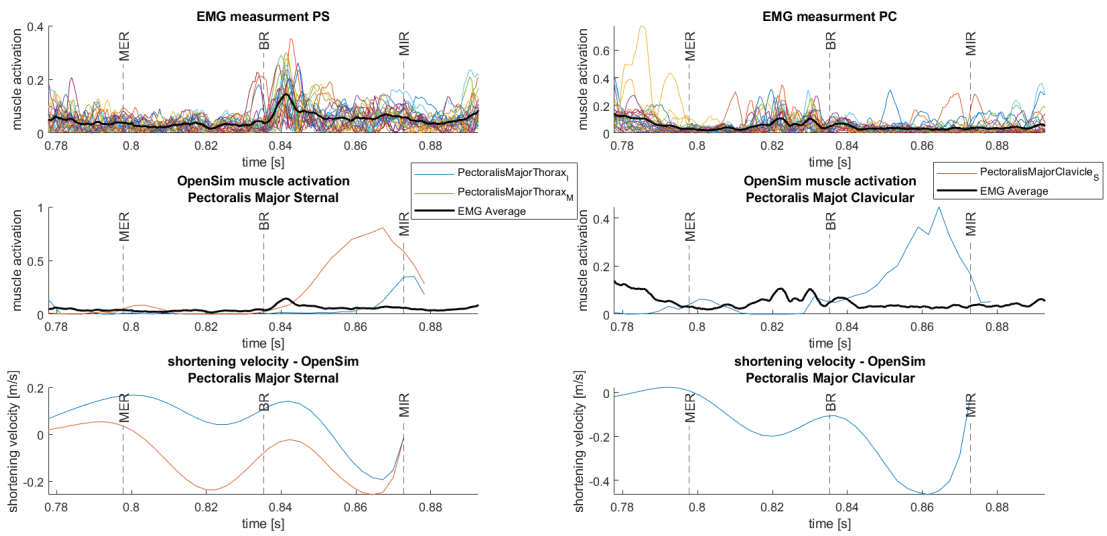


Figure 58: PP15: Comparison between muscle activity measured for Pectoralis Major and data obtained from static optimization, and fiber velocity computed based on the kinematics of the OpenSim model.

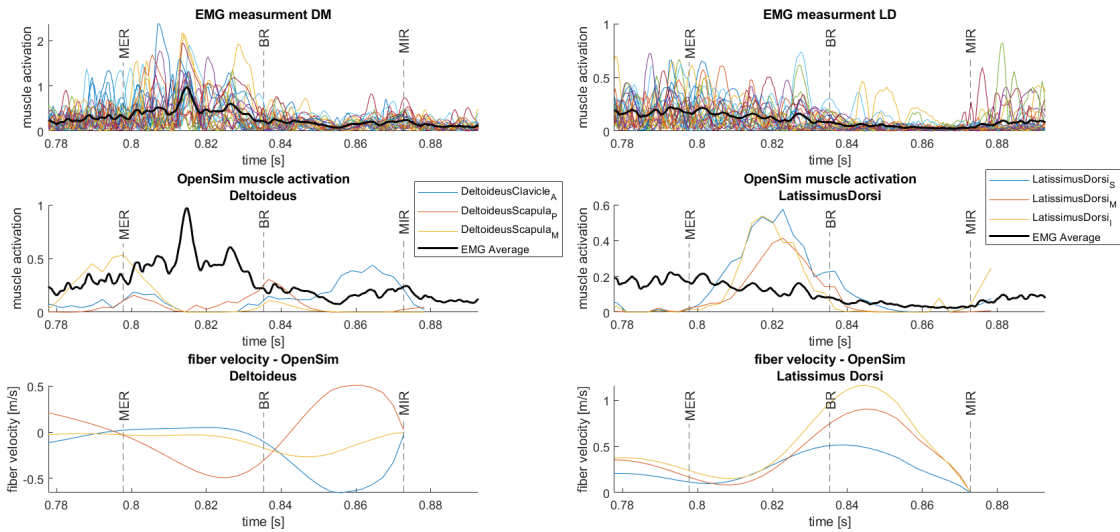


Figure 59: PP15: Comparison between muscle activity measured, for Deltoid muscle and Latissimus Dorsi, and data obtained from static optimization, and fiber velocity computed based on the kinematics of the OpenSim model.